Review article

Viktar S. Asadchy*, Ana Díaz-Rubio and Sergei A. Tretyakov

Bianisotropic metasurfaces: physics and applications

https://doi.org/10.1515/nanoph-2017-0132
Received December 22, 2017; revised January 23, 2018; accepted February 2, 2018

Abstract: Metasurfaces as optically thin composite layers can be modeled as electric and magnetic surface current sheets flowing in the layer volume in the metasurface plane. In the most general linear metasurface, the electric surface current can be induced by both incident electric and magnetic fields. Likewise, magnetic polarization and magnetic current can be induced also by external electric field. Metasurfaces which exhibit magnetoelectric coupling are called bianisotropic metasurfaces. In this review, we explain the role of bianisotropic properties in realizing various metasurface devices and overview the state-of-the-art of research in this field. Interestingly, engineered bianisotropic response is seen to be required for realization of many key field transformations, such as anomalous refraction, asymmetric reflection, polarization transformation, isolation, and more. Moreover, we summarize previously reported findings on uniform and gradient bianisotropic metasurfaces and envision novel and prospective research directions in this field.

Keywords: anomalous reflection; anomalous refraction; bianisotropy; chiral; metasurface.

1 Introduction

Despite the rich variety of known natural materials with different electromagnetic properties, we always explore new possibilities for material design to uncover all potential opportunities for applications. One straightforward solution to extend available properties of matter is to engineer atoms and molecules: their sizes, spatial distribution in the lattice, content as well as the electron cloud. Although this solution is not realistic at the atomic scale, it leads us to an idea of macro-engineering of matter constituents, which underlies the concept of metamaterials [1–4]. Metamaterials are composites of macroscopic "atoms" (meta-atoms) whose sizes are big enough to be easily fabricated and adjusted, and at the same time, small enough compared to the wavelength of incident radiation. Due to the subwavelength periodicity, metamaterials can be homogenized and described as ordinary materials with microscopic constituents.

During the last decade, two-dimensional counterparts of metamaterials, so-called metasurfaces, have been studied intensively (see reviews [5–14]). A metasurface represents an electrically thin composite material layer, designed and optimized to function as a tool to control and transform electromagnetic waves. The layer thickness is small and can be considered as negligible with respect to the wavelength in the surrounding space. In contrast to bulky metamaterials, metasurfaces do not require complicated three-dimensional fabrication techniques and suffer less from dissipation losses.

The concepts of metamaterials and metasurfaces are strongly associated with the notion of spatial dispersion [15–17]. Spatial dispersion effects occur when polarization in a specific location inside material depends not only on the local electric field at that location, but also on the field at other neighboring locations: a wave inside the material "feels" the structure of each atom (meta-atom). This effect is due to the finite sizes of meta-atoms and the finite wavelength of electromagnetic radiation, or equivalently, due to the finite speed of light. In natural materials, as a result of very small sizes of atoms and molecules compared to the wavelength of electromagnetic radiation (from radiowaves to ultraviolet), spatial dispersion can be observed only as weak effects of the order of 10^{-3} as compared with the locally induced electric polarization (e.g. optical activity of quartz) and smaller. Since in metamaterials and metasurfaces, the size of inclusions and the distances between them become comparable to the wavelength,

***Corresponding author: Viktar S. Asadchy,** Department of Electronics and Nanoengineering, Aalto University, P.O. Box 15500, FI-00076 Espoo, Finland; and Department of General Physics, Francisk Skorina Gomel State University, 246019 Gomel, Belarus, e-mail: viktar.asadchy@aalto.fi.
http://orcid.org/0000-0002-9840-4737
Ana Díaz-Rubio and Sergei A. Tretyakov: Department of Electronics and Nanoengineering, Aalto University, P.O. Box 15500, FI-00076 Espoo, Finland

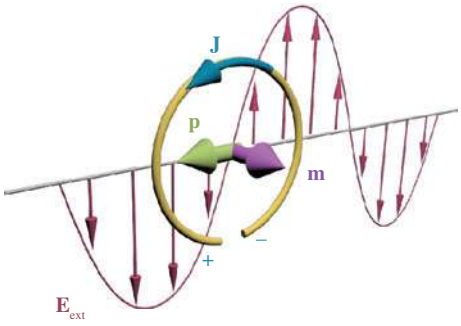

Figure 1: A metal split-ring resonator positioned in the electric field distribution $\mathbf{E}_{ext}$ of a standing wave. Since the resonator size is comparable to the wavelength, the induced polarization current **J** is nonlocal, i.e. depends on the external field in the whole volume occupied by the resonator. Due to the geometry of the split ring, electric field excites both the electric **p** and magnetic **m** dipoles.

composites constructed from them possess strong spatial dispersion, i.e. nonlocal polarization response. Figure 1 illustrates spatial dispersion effects by an example of a split-ring resonator illuminated by a standing wave. As is seen from the figure, the direction of polarization current (bound current induced due to polarization of the inclusion) at each point of the metal wire is not determined solely by the electric field at that point. Indeed, in the middle of the wire, the current is maximum, while the external electric field is zero.

The power of the metamaterial concept is in the ability to engineer the shapes and content of separate inclusions to control the polarization response of the composite in the most general fashion. By tailoring spatial dispersion in the composite, one can achieve two important phenomena. One of them, artificial magnetism, provides the possibility of creating materials with strong magnetic (diamagnetic or paramagnetic) properties in an arbitrary frequency range. This phenomenon opened the initial path for the rapid development of the field of metamaterials by enabling such paradigms as negative-index materials [1, 2, 18–20], invisibility cloak [21–24], subwavelength focusing [25, 26], and other.

The second phenomenon resulting from engineered spatial dispersion is bianisotropy [27]. Bianisotropic materials acquire magnetic (electric) polarization when excited by electric (magnetic) external field. Thus, term "bianisotropy" implies double ("bi-") polarization mechanism and anisotropic response. As is seen from Figure 1, a single split-ring resonator, in addition to electric and magnetic polarizations, also possesses bianisotropic response [28, 29] (electric field $\mathbf{E}_{ext}$ excites magnetic dipole moment **m**). Although first known study on bi-isotropic materials dates back to 1811 when François Arago observed rotation of the polarization plane of linearly polarized light in quartz, general properties for fields in bianisotropic media were understood only in 1970s [30], and wave propagation in bianisotropic media was extensively studied only in the 1990s [31–34]. During the last decade, the interest in bianisotropy has resumed thanks to the unique opportunities it provides for the design of metasurfaces: optical activity, asymmetric absorption and reflection, one-way transparency, anomalous refraction, etc. Moreover, bianisotropy is a stronger effect of spatial dispersion compared to artificial magnetism [31], which makes it an ideal candidate for achieving strong magnetic polarization at optical frequencies where magnetic response of conventional split-ring resonators saturates [35, 36].

Bianisotropy is not always attributed to spatial dispersion. Alternatively, nonreciprocal bianisotropic effects can be achieved, for example, in composites containing both magnetically and electrically polarizable components which are coupled via their reactive fields and experience influence of some external time-odd bias field or force [37–40]. Nonreciprocal bianisotropic metasurfaces can be used to design, for instance, various types of isolators with simultaneous control of amplitude and polarization of transmitted waves.

Despite recent growing interest to bianisotropic metasurfaces, to date, no systematic review of their principles of operation and applications has been presented. Thus, the goal of this work is to carry out in-depth analysis of physics of different bianisotropic effects in metasurfaces as well as to make an extensive overview of the known bianisotropic metasurfaces from the literature. Furthermore, the present paper aims to demonstrate the unique applications and functionalities which can be accomplished only with bianisotropic metasurfaces. The exposition of the content goes in the following order. Section 2 outlines the physics and features of different fundamental classes of bianisotropic meta-atoms. Section 3 provides a brief description of different homogenization models of bianisotropic metasurfaces. Finally, Sections 4 and 5 present an overview of earlier published works on uniform and gradient bianisotropic metasurfaces as well as classification of different functionalities they offer.

2 Bianisotropic meta-atoms

2.1 Reciprocal meta-atoms

The electromagnetic response of a homogenizable metasurface is determined by electric and magnetic dipole

moments induced in unit cells forming the metasurface. For a general linear meta-atom, the relations between the induced electric and magnetic dipole moments and the external fields existing at the position of the meta-atom are written as

$$\mathbf{p}=\bar{\bar{\alpha}}_{ee}\cdot\mathbf{E}_{loc}+\bar{\bar{\alpha}}_{em}\cdot\mathbf{H}_{loc},\ \mathbf{m}=\bar{\bar{\alpha}}_{me}\cdot\mathbf{E}_{loc}+\bar{\bar{\alpha}}_{mm}\cdot\mathbf{H}_{loc}, \quad (1)$$

where $\bar{\bar{\alpha}}_{ee}$, $\bar{\bar{\alpha}}_{mm}$, $\bar{\bar{\alpha}}_{em}$, and $\bar{\bar{\alpha}}_{me}$ are the electric, magnetic, electromagnetic, and magnetoelectric polarizability dyadics (or tensors) of the inclusion. Here the index "loc" indicates that if the meta-atom is positioned in an array, these fields are the local fields which excite this particular meta-atom. The local fields are created by external sources and the currents at all other meta-atoms which form the metasurface. If a single meta-atom is located in free space (not in an array), then the local fields are the incident fields measured at the position of the meta-atom.

Polarization response of atoms and molecules of natural nonmagnetic materials is predominantly determined by electric polarizability α_{ee}. Due to electrically small size of atoms ($a\ll\lambda$), the magnetoelectric α_{em}, α_{me} and magnetic α_{mm} polarizabilities are negligible, as weak spatial dispersion effects of a/λ and $(a/\lambda)^2$ orders. Atoms of magnetic materials exhibit additionally strong magnetic polarization response (not due to spatial dispersion), however, it occurs only at microwaves frequencies and below. General polarization response can be achieved in artificial meta-atoms with dimensions comparable to the wavelength. Engineering their shape and internal structure, one can enhance specific polarization effects, and in this case the magnitudes of the inclusion polarizabilities are not limited by $(a/\lambda)^m$ order (where $m=1, 2$).

The polarizability dyadics of particles made from linear materials obey the Onsager-Casimir symmetry relations [31, 41–45]. If the particles are reciprocal (that is, there is no external time-odd bias field nor external time modulation), they read

$$\bar{\bar{\alpha}}_{ee}=\bar{\bar{\alpha}}_{ee}^{T},\ \bar{\bar{\alpha}}_{mm}=\bar{\bar{\alpha}}_{mm}^{T},\ \bar{\bar{\alpha}}_{em}=-\bar{\bar{\alpha}}_{me}^{T}. \quad (2)$$

Here T denotes the transpose operation. These relations follow only from the time-reversal symmetry of Maxwell's equations and linearity of the particle response. Note that they are valid also for absorptive particles. It is seen that for reciprocal meta-atoms $\bar{\bar{\alpha}}_{me}$ is completely defined through $\bar{\bar{\alpha}}_{em}$.

The term "bianisotropic" refers to meta-atoms whose polarizability dyadics $\bar{\bar{\alpha}}_{em}$ and $\bar{\bar{\alpha}}_{me}$ are not zero and non-negligible. As is seen from (1), there are two basic scenarios of magnetoelectric coupling depending on the mutual orientation of the field ($\mathbf{E}_{loc}$ or $\mathbf{H}_{loc}$) and the dipole moment which is induced by this field (**m** or **p**, respectively). All other scenarios can be considered as a superposition of these two. The first scenario, where the moment and the field vectors are collinear, can be realized with a multiturn metallic three-dimensional helix [46–49] shown in Figure 2A. Under excitation by vertically oriented electric fields, the current induced in the wire forms a loop corresponding to a magnetic moment along the external electric field. The direction of the magnetic moment as well as the sign of the magnetoelectric polarizability depends on the helicity state of the helical inclusion. Such bianisotropic meta-atoms are called chiral meaning that they have broken mirror symmetry: a mirror image of the meta-atom cannot be superposed onto the original one by any operations of rotation and translation. Possible topologies of chiral meta-atoms at optical frequencies are plasmonic [50–52] and dielectric [31, 53, 54] multilayer patterns, as well as properly shaped plasmonic [55–58] and dielectric [59, 60] nanoparticles.

In the second scenario, the induced moment (e.g. **m**) and the field vector ($\mathbf{E}_{loc}$) are orthogonal. This can be realized by combining a loop and a straight electric dipole antenna, as shown in Figure 2B. This planar geometry, often referred to as the omega meta-atom [34, 61, 62] (after the Greek letter Ω), provides magnetoelectric polarization orthogonal to the exciting field. The sign of the magnetoelectric polarizability can be reversed by twisting the loop of the inclusion at 180° [63]. A split-ring resonator is a special case of the omega inclusion depicted in Figure 2B. At optical frequencies, omega meta-atoms can be implemented with both plasmonic [35, 64, 65] and dielectric [66, 67] materials.

The aforementioned scenarios define two basic functionalities of reciprocal bianisotropic metasurfaces composed of meta-atoms: polarization rotation and asymmetric scattering (see detailed discussion in Section 4). However, to achieve these functionalities, it is not

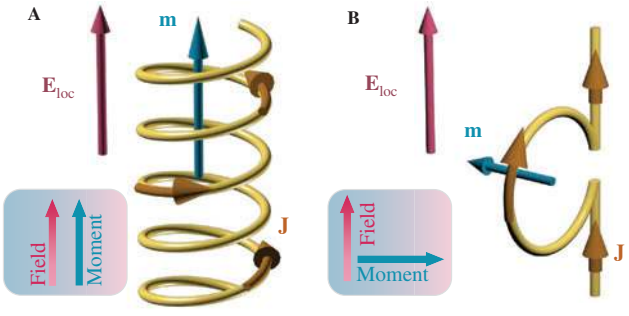

Figure 2: Topologies of two basic reciprocal bianisotropic inclusions. (A) A chiral metal inclusion with the shape of a true helix and (B) an omega inclusion with shape of the Ω letter.

necessary to use the meta-atoms shown in Figure 2. In fact, an inclusion of a general shape can act as chiral and omega meta-atoms for different illuminations. Indeed, an arbitrary electromagnetic dyadic $\bar{\bar{\alpha}}_{\text{em}}$ can be always decomposed into a linear combination of three basic dyadics [31, 68–71]:

$$\bar{\bar{\alpha}}_{\text{em}} = T\bar{\bar{I}} + \sum_{i=1}^{3} P_i \mathbf{a}_i \mathbf{a}_i + A(\mathbf{b}\times\bar{\bar{I}}), \tag{3}$$

where T, P_i and A are complex amplitudes defining the weights of each dyadic in the linear combination, $\bar{\bar{I}}$ is the unit dyadic, $\mathbf{a}_i$ and $\mathbf{b}$ are unit vectors [72] (the directions that they define are clarified below). The first term in (3) defines isotropic true (or intrinsic) chiral bianisotropic response. It is not zero only for meta-atoms with broken mirror symmetry. One can model this response, as is shown in Figure 3A, by the response of three helices of the same helicity state arranged with equal density along the Cartesian basis unit vectors in a lattice. The dimensions of the helices define amplitude T. A true chiral meta-atom (the three helices) exhibits chiral effects (polarization rotation, circular dichroism, etc.) when illuminated from an arbitrary direction. It should be noted that true chirality can be achieved only with three-dimensional meta-atoms.

The second term in (3) refers to the so-called pseudochiral (or extrinsic) bianisotropic response. In the lossless case it can be modeled by three metal helices oriented along the basis vectors $\mathbf{a}_i$ with the strengths of electromagnetic coupling determined by amplitudes P_i (see Figure 3B). The sum of all amplitudes P_i must be equal to the trace of the second dyadic in composition (3), i.e. equal to zero. This implies that the helices oriented along the basis vectors $\mathbf{a}_i$ must be of different handedness so that in total true chirality in the entire inclusion (unit cell) is compensated. Importantly, although pseudochiral bianisotropic inclusions do not possess true chiral electromagnetic response, they do exhibit chiral effects for certain illumination directions, namely along the eigenvectors $\mathbf{a}_i$. This fact has led to far-reaching implications, enabling to achieve various chiral effects even with planar (two-dimensional) structures suitable for various nanofabrication techniques [68, 73–78].

Finally, the last (antisymmetric) term in (3) represents omega bianisotropic coupling. A uniaxial omega meta-atom (formed by two orthogonal omega-shaped inclusions) shown in Figure 3C oriented along vector $\mathbf{b}$ models such electromagnetic coupling. Illuminated along the $-\mathbf{b}$ and $+\mathbf{b}$ directions, the omega meta-atom possesses asymmetric scattering toward the direction of the source.

The universality of the described classification of reciprocal bianisotropic meta-atoms can be demonstrated by an example of an arbitrary inclusion with a given electromagnetic tensor $\bar{\bar{\alpha}}_{\text{em}}$:

$$\bar{\bar{\alpha}}_{\text{em}} = -\frac{jV}{c}\begin{bmatrix} 2 & 1 & 0 \\ 1 & 2 & -1 \\ 0 & 1 & 2 \end{bmatrix}, \tag{4}$$

where V is the volume of the meta-atom, c is the speed of light in vacuum and j is the imaginary unit. Throughout the paper, time-harmonic dependency in the form $e^{j\omega t}$ is assumed. From (3), the following amplitudes can be found: $T=-2jV/c$, $P_1=jV/c$, $P_2=0$, $P_3=-jV/c$, $A=-jV/c$. The eigenvectors are given in terms of the original basis vectors as $\mathbf{a}_1=[-1;\ 1;\ 0]^T$, $\mathbf{a}_2=[0;\ 0;\ 1]^T$, and $\mathbf{a}_3=[1;\ 1;\ 0]^T$, while vector $\mathbf{b}$ is equal to $[1;0;0]^T$. Therefore, properties of the meta-atom with bianisotropic tensor (4) can be described by the decomposition depicted in Figure 3D. As is seen from the figure, now the electromagnetic response is easily determined for different illumination directions. For example, the maximum chiral effect appears when incident wave propagates along the bisection of the angle between the $-x$ and $+y$ axes because in this scenario the

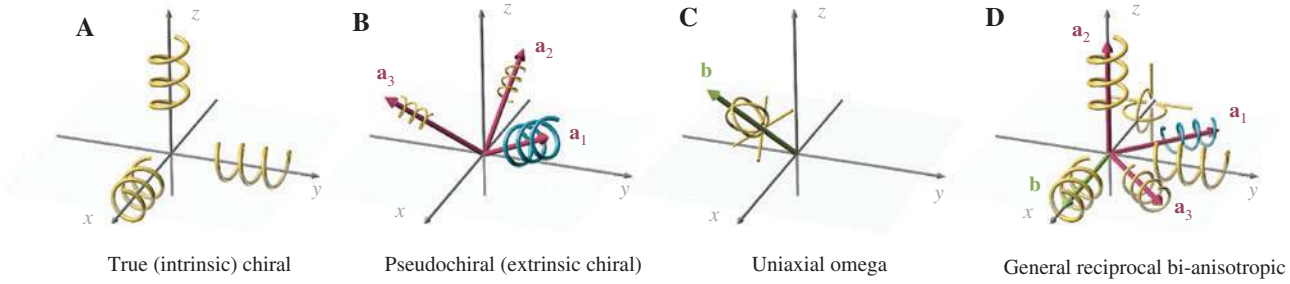

Figure 3: Conceptual realizations of basic reciprocal bianisotropic meta-atoms.
(A) True (or intrinsic) chiral meta-atom. (B) Pseudochiral (extrinsic) meta-atom. The right- and left-handed helices are shown in yellow and blue, respectively. Different size of the helices corresponds to the different amplitudes of polarizabilities. (C) Uniaxial omega meta-atom. (D) The conceptual representation of the bianisotropic meta-atom with electromagnetic coupling described by (4).

left-handed helix (shown in blue) is not excited, while the other three right-handed helices are activated. Furthermore, the highest asymmetry of backscattering occurs when the virtual omega inclusion is excited, i.e. for incident waves propagating along the $\pm x$-axis.

The problem of finding proper geometrical parameters of a bianisotropic meta-atom knowing its required polarizabilities is not trivial. In some simple cases, it is possible to roughly determine the dimensions and material characteristics of the inclusions based on known theoretical models [47, 79]. However, in most cases of bianisotropic inclusions, the correspondence between their polarizabilities and internal structure can be set up only with the use of numerical and semi-analytical techniques (see e.g. [80–83]).

2.2 Nonreciprocal meta-atoms

Materials and their constituents that possess different electromagnetic response under time reversal are called nonreciprocal. To break the time-reversal symmetry, there must be some external perturbations acting on the material, because the microscopic and macroscopic Maxwell equations are symmetric under time reversal. Such perturbations can be of nonelectromagnetic as well as electromagnetic nature. A good example is an external static magnetic field bias. Materials such as metals and ferromagnetics placed in external magnetic field would exhibit different response for different directions of time flow in the system. The magnetic bias field is assumed to be invariant to the time flow since it is external to the considered system. Other examples of nonreciprocal materials are magnetized plasma and magnetized graphene. Nonreciprocal response can be achieved also by other means: materials moving with some speed, magnetless active materials mimicking electron spin precession of natural magnets [37, 84–86], nonlinear materials [38], time-modulated materials [87].

Nonreciprocal meta-atoms (namely those biased by some external force) can be engineered to exhibit nonreciprocal bianisotropic response. For such meta-atoms, the polarizability dyadics can be introduced as in (1). The Onsager-Casimir symmetry relations have the form [41–43]:

$$\begin{aligned}\bar{\bar{\alpha}}_{\mathrm{ee}}(\mathbf{H}_0)=\bar{\bar{\alpha}}^{T}_{\mathrm{ee}}(-\mathbf{H}_0),\quad \bar{\bar{\alpha}}_{\mathrm{mm}}(\mathbf{H}_0)=\bar{\bar{\alpha}}^{T}_{\mathrm{mm}}(-\mathbf{H}_0),\\ \bar{\bar{\alpha}}_{\mathrm{em}}(\mathbf{H}_0)=-\bar{\bar{\alpha}}^{T}_{\mathrm{me}}(-\mathbf{H}_0),\end{aligned} \tag{5}$$

where $\mathbf{H}_0$ denotes all external nonreciprocal parameters (e.g. bias magnetic field) and $-\mathbf{H}_0$ corresponds to the case when all these parameters switch signs.

Similarly to the above consideration for reciprocal meta-atoms, one can distinguish two basic nonreciprocal bianisotropic inclusions based on the mutual orientation of the local field $\mathbf{E}_{\mathrm{loc}}$ and the dipole moment $\mathbf{m}$ induced by this field. In the first scenario, when $\mathbf{E}_{\mathrm{loc}}$ and $\mathbf{m}$ are collinear, an example appropriate geometry of the inclusion is shown in Figure 4A. It consists of a ferrite sphere (here, ferrite is chosen since it is nonconductive in contrast to other magnetic alloys) magnetized by external magnetic field $\mathbf{H}_0$ and located in the proximity of metal wires of a cross shape. The electric field of the incident wave excites the electric current along the wires which, in turn, excites alternating magnetic field around the wires. This magnetic field induces a magnetic moment in the ferrite sphere. Likewise, the incident magnetic field excites an electric dipole moment in the wires through magnetization of the sphere. The inclusion shown in Figure 4A was theoretically studied in [40, 88, 89] and experimentally tested in [90]. It was named Tellegen meta-atom after Bernard Tellegen who suggested the first prototype of such an inclusion [39].

The topology of the inclusion corresponding to the second scenario, when the local field and the induced moment are orthogonal, is shown in Figure 4B. Such inclusion is sometimes named as an artificial moving atom [40] since a composite of such meta-atoms exhibits the same electromagnetic response as that of an ordinary isotropic material which is truly moving with some speed. The first analytical study on polarizabilities of nonreciprocal bianisotropic inclusions was reported in [91]. Interestingly, it appears that no realizations of nonreciprocal bianisotropic meta-atoms at optical frequencies are known. This interesting and challenging area remains completely unexplored.

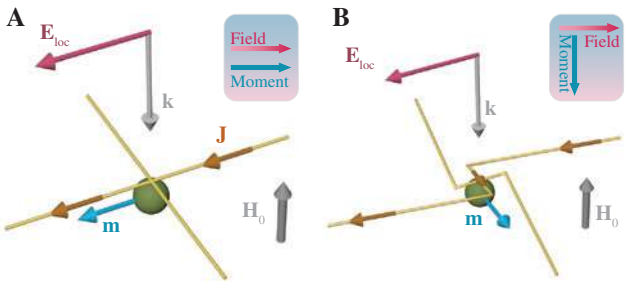

Figure 4: Topologies of nonreciprocal bianisotropic inclusions. (A) Uniaxial Tellegen inclusion. (B) Uniaxial artificial moving inclusion. The ferrite sphere is shown in green. The inclusions are excited by an incident electric field $\mathbf{E}_{\mathrm{loc}}$. For clarity, magnetic moments $\mathbf{m}$ induced due to only nonreciprocal bianisotropic effects are shown. Note that these inclusions do not exhibit pure nonreciprocal response and possess also reciprocal effects of chiral and omega couplings.

It is important to mention that nonreciprocal bianisotropic coupling is not an effect of spatial dispersion. In contrast to reciprocal spatially dispersive inclusions where magnetoelectric and magnetic response can occur only due to their finite sizes, nonreciprocal inclusions exhibit these responses even in locally uniform external fields (when the particle size is negligibly small compared to the wavelength). For example, in the considered ferrite-based inclusions, uniform electric field excites electric current in the wires which in turn induce magnetic moments in the ferrite sphere. Thus, generally, bianisotropic properties of a medium can be caused by two distinguished effects: reciprocal spatial dispersion effects and nonreciprocal magnetoelectric coupling.

2.3 Maximizing bianisotropy

In many applications of bianisotropic meta-atoms, it is required to bring their magnetoelectric properties to the balance with the electric and magnetic ones. Such bianisotropic meta-atoms (both reciprocal and nonreciprocal) are called optimal or balanced and their main polarizability components satisfy the relation [92–94]:

$$|\eta_0\alpha_{ee}|=|\alpha_{em}|=\left|\frac{1}{\eta_0}\alpha_{mm}\right|, \tag{6}$$

where η_0 is the wave impedance of free space. In particular, it was demonstrated that balanced chiral particles do not interact with the waves of one of the two circular polarizations at all, maximizing the effects of optical dichroism [92, 94, 95]. Condition (6) also appears for bianisotropic meta-atoms realizing various polarization transformations [48, 96], cloaking [97], zero forward and backward scattering [98, 99], total absorption [100], one-way transparency [101], etc. Moreover, the balanced meta-atoms extract/radiate maximum power from the incident electromagnetic fields (for a given overall size and the resonant frequency of the inclusion) [93].

Previously, relation (6) was considered as an upper limit for the strength of bianisotropic coupling $|\alpha_{em}|$ in meta-atoms [32, 47, 102, 103]. The recent study [104] demonstrated that by decoupling the electric and magnetic modes in the meta-atom, one can largely maximize the bianisotropic effects ($|\alpha_{em}|\gg|\alpha_{ee}|$ and $|\alpha_{em}|\gg|\alpha_{mm}|$). Analogous giant bianisotropic properties can be achieved in bulk materials (so-called bianisotropic nihility) [71, 105–107].

3 Homogenization of bianisotropic metasurfaces

Metasurface is a two-dimensional array of meta-atoms. An engineered composite structure forming a metasurface is assumed to behave as an effectively homogeneous sheet in the electromagnetic (optical) sense, meaning that it can be considered continuous on the wavelength scale. Thus, the metasurface can be adequately characterized by its effective, surface-averaged properties. In the strict sense of the homogenization models, if the effective parameters vary over the surface, it is assumed that the variations are slow at the wavelength scale. That is, it is assumed that there are at least several elements (often called meta-atoms) in every area of the size $\lambda\times\lambda$, and the polarizations of these meta-atoms are nearly the same. However, many metasurfaces work in the mesoscopic regime where there are only a few inclusions per wavelength along the surface. Nevertheless, homogenized models provides most useful physical insight and approximate design guidelines even in this situation.

Similarly to volumetric materials, where the notions of the permittivity and permeability result from volumetric averaging of microscopic currents over volumes which are small compared to the wavelength, the metasurface parameters result from two-dimensional surface averaging of microscopic currents at the same wavelength scale. Since the physical assumptions under the homogenization models of metasurfaces and metamaterials are the same, metasurfaces are sometimes defined as two-dimensional versions of metamaterials.

Illuminated by an incident wave, the inclusions of the metasurface acquire electric and magnetic polarizations which can be expressed via the corresponding dipole moments (see Figure 5A). Homogenization implies that the discrete array of dipole moments is modeled by an

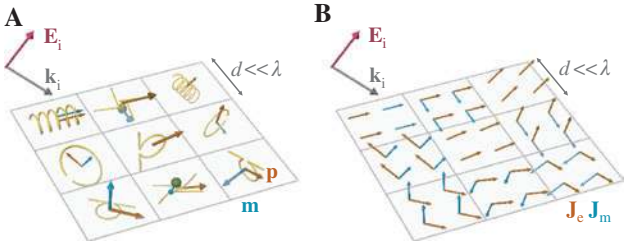

Figure 5: Homogenization of nonuniform metasurfaces. (A) A metasurface consisting of arbitrary subwavelength inclusions. An incident wave excites certain electric **p** and magnetic **m** dipole moments in the meta-atoms. (B) Modeling the actual metasurface by an array of continuous sheets with averaged over the unit cell electric $\mathbf{J}_e$ and magnetic $\mathbf{J}_m$ currents.

array of unit cells with continuous surface-averaged currents $\mathbf{J}_e$ and $\mathbf{J}_m$ shown in Figure 5B. These currents can be found as the time derivatives of the electric and magnetic polarization densities. These densities, in turn, equal to surface-averaged electric and magnetic dipole moments of meta-atoms. Finally, the relations between the averaged surface currents and the electric and magnetic moments read

$$\mathbf{J}_e = \frac{j\omega \mathbf{p}}{S}, \quad \mathbf{J}_m = \frac{j\omega \mathbf{m}}{S}, \tag{7}$$

where S is the unit-cell area. The current flow produces discontinuities of the tangential components of the fields at both sides of the metasurface which can be expressed as [108–111]

$$\mathbf{n} \times (\mathbf{H}_t^+ - \mathbf{H}_t^-) = \mathbf{J}_e, \quad \mathbf{n} \times (\mathbf{E}_t^+ - \mathbf{E}_t^-) = -\mathbf{J}_m. \tag{8}$$

Here, "+" and "−" superscripts denote the two half-spaces at the two sides of the metasurface. The respective fields represent combinations of the incident field and the scattered fields by the metasurface. The unit normal vector $\mathbf{n}$ points from half-space " − " to half-space " + ".

Relations (8) do not describe the properties of the metasurfaces, they only determine the tangential field jumps if the surface currents are known, and vice versa. To engineer metasurface response defined by the scattered fields, it is required to control the surface currents, and consequently, the electric and magnetic polarizations in the metasurface. There are several conventional models for characterization of metasurface response to incident fields in terms of its macroscopic parameters: models based on polarizabilities [112–117] and susceptibilities [111, 118–121] of metasurface inclusions, equivalent impedance matrix model [122–126], and diffractive interface model [127].

Polarizabilities relate polarizations in a metasurface with the local fields which cause these polarizations. The local fields at the position of a particular metasurface inclusion are defined as $\mathbf{E}_{loc} = \mathbf{E}_i + \overline{\overline{\beta}}_e \cdot \mathbf{p}$ and $\mathbf{H}_{loc} = \mathbf{H}_i + \overline{\overline{\beta}}_m \cdot \mathbf{m}$, where $\overline{\overline{\beta}}_e$ and $\overline{\overline{\beta}}_m$ are the interaction constant dyadics that describe the effect of the entire metasurface on a single inclusion. This approach allows one to express the electric and magnetic dipole moments of a single inclusion in terms of known incident fields $\mathbf{E}_i$ and $\mathbf{H}_i$ as

$$\mathbf{p} = \overline{\overline{\hat{\alpha}}}_{ee} \cdot \mathbf{E}_i + \overline{\overline{\hat{\alpha}}}_{em} \cdot \mathbf{H}_i, \quad \mathbf{m} = \overline{\overline{\hat{\alpha}}}_{me} \cdot \mathbf{E}_i + \overline{\overline{\hat{\alpha}}}_{mm} \cdot \mathbf{H}_i, \tag{9}$$

where the dyadics with hats denote effective or collective polarizabilities which characterize the properties of individual inclusions and their interactions in the lattice [112–117]. The polarizability-based model provides not only information about the macroscopic response of the array, but also about the individual response of the constituent elements giving a straightforward way to determine what kind of particle should be used to obtain a specific electromagnetic response.

By contrast, there are other homogenization models based on the macroscopic characteristics of the metasurface. For example, the susceptibility-based model relates the polarization moments with the electric $\mathbf{E}_{av}$ and magnetic $\mathbf{H}_{av}$ fields averaged over the two sides of the metasurface. In this case the electric and magnetic dipole moments read $\mathbf{p} = S\varepsilon_0 \overline{\overline{\chi}}_{ee} \cdot \mathbf{E}_{av} + S\sqrt{\varepsilon_0 \mu_0}\, \overline{\overline{\chi}}_{em} \cdot \mathbf{H}_{av}$ and $\mathbf{m} = S\overline{\overline{\chi}}_{me} \cdot \mathbf{E}_{av} + S\sqrt{\varepsilon_0 / \mu_0}\, \overline{\overline{\chi}}_{mm} \cdot \mathbf{H}_{av}$, where dyadic $\overline{\overline{\chi}}$ denotes macroscopic surface-averaged susceptibilities (SI metric units) [111, 118–121]. The main advantage of the homogenization model based on the macroscopic surface susceptibility tensors is that, knowing a specific tensor, one can immediately see if the metasurface inclusions must be lossy or possess some gain.

An alternative homogenization model for metasurfaces can be established based on the analogy between plane-wave propagation in free space and signal propagation in a transmission line. The electromagnetic fields propagating in free space can be referred to voltages and currents of signals propagating in a transmission line related by an equivalent impedance matrix [122–126]. The method presents several advantages. First of all, when the fields at both sides of the metasurface are specified, one can calculate the impedances and extract the following information: whether metasurface should be capacitive or inductive, lossy or active, reciprocal or nonreciprocal, symmetrical or nonsymmetrical, etc. Second, based on the transmission-matrix approach, one can easily determine reflection/transmission properties of the metasurface.

4 Uniform bianisotropic metasurfaces

4.1 Early works

Metasurfaces as thin composite layers formed by subwavelength unit cells have been studied for a very long time, well before the term metasurface has been coined. Perhaps the most studied and practically interesting example is a dense mesh of metal wires or strips. In 1898, H. Lamb showed that by varying the ratio between the wire radius and the period, it is possible to tune the reflectivity

from nearly zero to nearly unity [128]. Analytical homogenized models of single-layer arrays of conducting wires and strips are well developed, including the case of sparse grids [129].

One of the early examples of bianisotropic metasurfaces is the high-impedance surface in form of a dense array of metal patches over a ground plane [130]. The reflection coefficients of the two sides of this metasurface are obviously different, which suggests that the metasurface exhibits omega-type bianisotropic coupling. Indeed, this is the case: in [131], the bianisotropic coupling coefficient for such high-impedance surface was analytically calculated. Accurate dynamic models of high-impedance surfaces are available in [132, 133], and more complex effects of spatial dispersion in these structures have been studied in [134]. Engineering reactive fields close to small resonant inclusions allows dramatic reduction of the metasurface thickness [135]. An interesting early example of a resonant bianisotropic metasurface is an array of small conducting spirals at a metal ground plane [136]. Besides omega bianisotropy, this structure possesses very strong resonant magnetic properties, such that the effective permeability of the layer becomes negative.

In the array of helices in [136], resonant spirals were arranged in a racemic array, so that the metasurface did not exhibit chiral effects. Reflections from chiral metasurfaces formed by long (nonresonant) spirals were studied in [137]. In addition, properties of single and double arrays of small bianisotropic particles were studied in papers [112, 122] and other works before metasurfaces had been conceptualized.

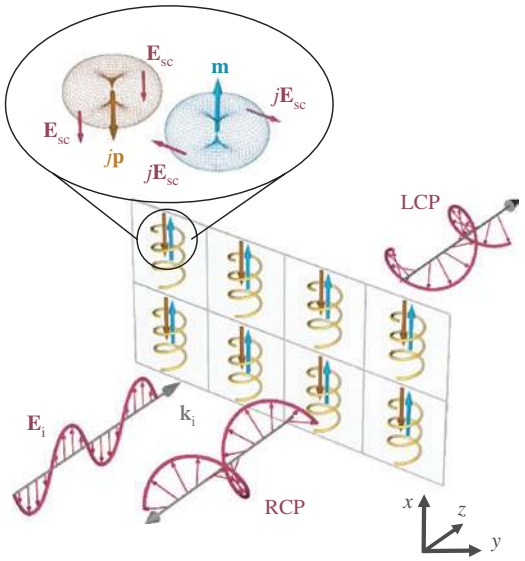

Figure 6: Electromagnetic response of a basic metasurface formed by chiral right-handed balanced inclusions. The inset depicts the radiation patterns of the electric and magnetic dipole moments. Linearly polarized incident electric field $\mathbf{E}_i$ excites electric $\mathbf{p}$ and magnetic $j\mathbf{m}$ dipole moments in the inclusions which in turn radiate scattered waves denoted as $\mathbf{E}_{sc}$ and $j\mathbf{E}_{sc}$. Thus, the metasurface completely reflects RCP-component of the incident wave and transmits the LCP-component.

4.2 Polarization transformers

4.2.1 Circular-polarization-selective surfaces

A large variety of devices for polarization transformations can be built based on chiral metasurfaces. To demonstrate it, let us consider a metasurface composed of chiral bianisotropic helices oriented along one direction as shown in Figure 6. An incident plane wave with the *x*-oriented electric field $\mathbf{E}_i$ induces both $\mathbf{p}$ and $\mathbf{m}$ moments in each helix along the *x*-axis (see also Figure 2A). The incident magnetic field does not excite the helices, and therefore, according to (9), the amplitudes and phases of the induced dipole moments are determined solely by the electric $\hat{\alpha}_{ee}$ and magnetoelectric $\hat{\alpha}_{me}$ polarizabilities of the helices, respectively. In particular, these polarizabilities can have equal amplitudes and 90° phase difference, i.e. $j\hat{\alpha}_{ee} = \hat{\alpha}_{me}$ [96], resulting in the same phase shift between the electric and magnetic dipole moments (the phase shift is indicated in the figure by an imaginary unity *j*). Figure 6 illustrates scattering from a metasurface in this case. The electric and magnetic dipole moments radiate plane waves with orthogonal linear polarizations. The fields of these waves can be determined using (7) and (8). Due to the phase shift of 90° between two linearly polarized waves, the resulting scattered wave (in both forward and backward directions) is circularly polarized with the same handedness as that of the helices. Thus, if the helices are right-handed, the reflected wave has right-handed circular polarization (RCP). At the same time, polarization of the transmitted wave (created by the interference of the incident and forward scattered waves) is left-handed circular (LCP). Thus, such a chiral metasurface transmits one circular polarization and completely reflects (alternatively absorbs) another one. This functionality called circular polarization selectivity or circular dichroism (in the case of absorption) is the basis for various polarization filters. It should be noted that circular polarization selectivity can be viewed also as an effect of polarization transformation (from linear to circular). Obviously, the efficiency of such polarization transformation is limited by 50%. The response of an ideal circular-polarization-selective surface can be easily visualized with the corresponding Jones matrix:

$$\bar{\bar{S}}_{21} = \frac{e^{j\vartheta}}{2}\begin{pmatrix} 1 & j \\ -j & 1 \end{pmatrix}, \tag{10}$$

where ϑ is an arbitrary phase.

Polarization selectivity is a well-known and explored phenomena. It can be found in nature: for example, the exoskeleton of scarab beetles selectively reflects left circularly polarized light [138, 139]. The polarization selectivity is caused by the chiral (mirror-asymmetric) structure of the cells in the exoskeleton. The first artificial circular-polarization-selective device was proposed in 1966 [140]. The structural unit cell (shown in Figure 7A) consisted of a bent wire with the overall length of λ (operating wavelength). The wire was bent into a crank-like shape possessing broken mirror symmetry. The same design was independently rediscovered by Morin [144]. A short review on circular-polarization-selective surfaces by the year 1996 can be found in [141].

Observation 1. *To design a circular-polarization-selective reciprocal surface (such that the transmission coefficients for RCP and LCP light are not equal), it must necessarily possess true or pseudochiral properties* (the proof can be made based on Section IV of [96]). This also implies that reciprocal anisotropic metasurfaces cannot exhibit asymmetric transmission of circularly polarized light of opposite handedness. However, to design such a metasurface, it is not required to use disconnected helical-like inclusions [96] as those shown in the conceptual example in Figure 6. An attractive alternative to realize a chiral polarization-selective metasurface was described in [142, 145]. It was demonstrated that a chiral metasurface can be synthesized by cascading several anisotropic patterned metallic sheets (electric sheet admittances) twisted one with respect to another (see Figure 7B). Indeed, a transfer matrix (*ABCD*-matrix) of a cascade of the sheet admittances can be properly engineered to achieve desired *S*-parameters of the metasurface. Figure 7B (right) depicts simulated transmission of LCP and RCP waves through a cascade of rotated anisotropic sheets. It is seen that in the wide frequency band the metasurface exhibits asymmetric transmission for circularly polarized incident waves of opposite handedness. The same idea of cascading electrically polarizable anisotropic patterns was exploited in [143, 146, 147]. The authors of these works proposed a systematic approach to design a metasurface with general reciprocal bianisotropic

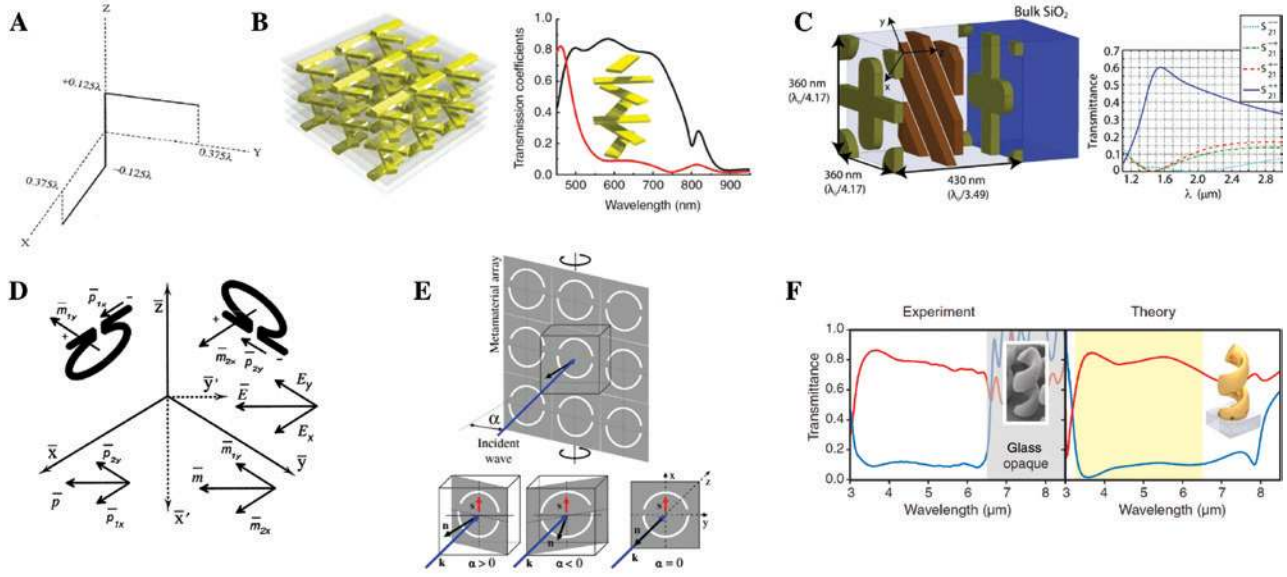

Figure 7: Circular-polarization-selective metasurfaces.
(A) Design for Pierrot's unit cell of an artificial circular-polarization-selective surface. Reprinted figure from [141]. Copyright (1996) by IEEE. (B) Left: Illustration of a cascade of stacked patterned metallic sheets twisted one with respect to another. Right: Transmission coefficients of LCP (red line) and RCP (black line) waves through the cascade. The inset illustrates one unit cell of the metasurface. Reprinted figure from [142]. Copyright (2012) by Springer Nature. (C) Left: Unit cell consisted of three patterned sheets. Right: Transmittance on a linear scale ($|S_{21}|^2$), where the superscript + denotes RCP and – denotes LCP light. Reprinted figure from [143]. Copyright (2014) by the American Physical Society. (D) Explanation of the microscopic chiral effect in a metasurface composed of planar inclusions. Reprinted figure from [68]. Copyright (1997) by Springer Nature. (E) A planar pseudochiral metasurface exhibiting circular dichroism at oblique incidence of light. Reprinted figure from [78]. Copyright (2009) by the American Physical Society. (F) Normal-incidence measured and theoretically calculated transmittance spectra for LCP (red) and RCP (blue) light through an array of right-handed metallic helices. Reprinted figure from [55]. Copyright (2009) by the AAAS.

properties. The engineered structure consisted of three admittance sheets separated by subwavelength distances as shown in Figure 7C. The geometry of the sheet pattern was determined using the theory of frequency-selective surfaces [148]. The transmission coefficients for LCP and RCP waves are shown in Figure 7C. It can be seen that, at the design frequency, the metasurface achieved low loss for RCP infrared light and provided great isolation for LCP light. Chiral response can be also achieved in a cascade of two sheets with both electric and magnetic polarizations [149]. Interestingly, quite similar ideas were developed earlier in crystalloptics, where chiral structures were realized as superlattices formed by rotated layers of uniaxial crystals, see [31], Section 9.5].

A circular-polarization-selective response can be achieved even with a metasurface which is not truly chiral. Indeed, as it was discussed in Section 2.1, even mirror-symmetric (pseudochiral) meta-atoms might exhibit chiral effects when illuminated from specific directions (similarly to those denoted as $\mathbf{a}_i$ in Figure 3). For the first time, detailed theoretical analysis of this effect was reported in [68]. Figure 7D explains the existence of chiral effect in a unit cell composed of planar (nonchiral) omega meta-atoms. For the specific orientation of electric field **E** shown in the figure, the induced total magnetic moment $\mathbf{m}=\mathbf{m}_{1y}+\mathbf{m}_{2x}$ is parallel to it, resembling the scenario shown in Figure 2A. The first experimental demonstration of a circular-polarization-selective metasurface based on pseudochiral (extrinsically chiral) inclusions was independently reported in [77, 78, 150–152]. The metasurface comprised planar meta-atoms lacking an inversion center, i.e. possessing a polar direction (denoted as **s** in Figure 7E). When illuminated at normal incidence ($\alpha=0$), such inclusions do not exhibit chiral properties. However, the metasurface becomes optically active at oblique incidence provided that the plane of incidence does not contain the polar direction.

Another mechanism of circular-polarization selectivity relies on combination of internal and Bragg resonances in a single metasurface with helical inclusions of wavelength scale [55]. Strictly speaking, such a metasurface structure can be considered as a diffraction grating. In contrast to above considered examples, this structure operates for illumination along the axis of the helices. The transmittance spectra for LCP and RCP light are shown in Figure 7F, revealing circular polarization selectivity.

4.2.2 Polarization rotators

Polarization rotation or optical activity phenomenon has been studied for the first time by French scientists Arago (1811) and Biot (1812) [32]. Linearly polarized light passed through optically active material experiences polarization rotation since RCP and LCP components of light travel through the material with different speeds (circular birefringence). This response is described by the following Jones matrix (for the uniaxial case):

$$\overline{\overline{S}}_{21}=e^{j\vartheta}\begin{pmatrix}0 & -1\\ 1 & 0\end{pmatrix}. \tag{11}$$

Conventional ways of engineering planar polarization rotators are based on cascades of wire-grid polarizers whose wires are oriented in different directions in different layers [153–155] or optically anisotropic planar arrays of meta-atoms [156, 157]. The main drawback of these approaches is that the structure works only for a certain polarization of incident waves. The same conclusion applies to known pseudochiral metasurfaces operating at oblique angles [151]. This problem can be overcome by using a cascade of two dielectric half-wave plates with crystal axes rotated by 45° relative to each other. However, dielectric half-wave plates are available only for certain frequency ranges and result in devices with thicknesses comparable to the wavelength, which is undesirable for their integration in nanophotonic systems.

Observation 2. *To realize a polarization rotating subwavelength-thin reciprocal metasurface insensitive for polarization of incident waves (at normal incidence), nonzero chirality is a necessary condition and the inclusions must be uniformly distributed in the metasurface plane* [96]. This is in sharp contrast to the case shown in Figure 6 where all the inclusions were aligned along one direction. Due to uniformly distributed inclusions and their balanced electric and magnetic properties, reflections can be completely suppressed. The first metasurface exhibiting uniaxial polarization rotation consisted of a stack of slightly tilted metallic strips [158] shown in Figure 8A. The chirality of the meta-atom is nonzero because it cannot be superposed with its mirror image. The meta-atoms are of the same handedness and randomly oriented in the metasurface plane.

Alternatively, uniaxial polarization rotation can be achieved with chiral metasurfaces whose constituents possess fourfold rotational symmetry [50, 159, 161–166] such as that shown in Figure 8B. Typically, these structures provide high efficiency up to 90% (see Figure 8B); however, their design requires intensive optimization processes. In contrast, the authors of [58, 96, 167] proposed almost fully analytical synthesis of the metasurface for polarization rotation. This was accomplished via unit cells with canonical helical inclusions as that shown in Figure 8C. The efficiency of such metasurfaces is limited only

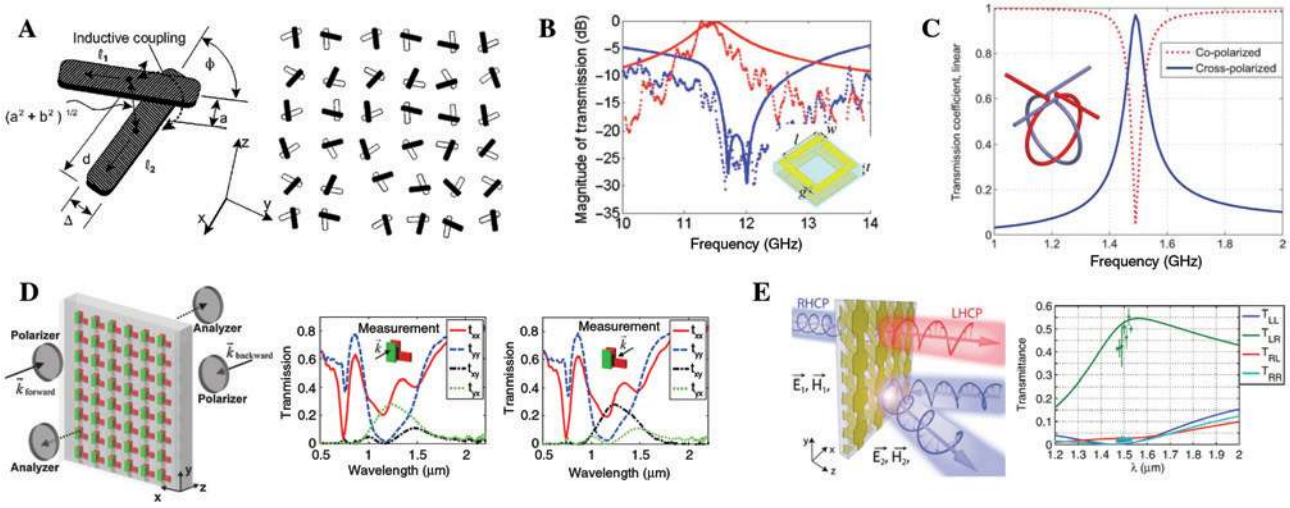

Figure 8: Metasurfaces for polarization rotation and asymmetric transmission.
(A) A unit cell (left) and a bilayered planar chiral metasurface based on it with inductive cross-layer coupling (right). Reprinted figure from [158]. Copyright (2001) by AIP Publishing. (B) Transmission spectra for co- (blue) and cross-polarized (red) light. Simulated and measured data are shown as solid and dotted lines, respectively. The inset shows the metasurface unit cell with fourfold rotational symmetry. Reprinted figure from [159]. Copyright (2010) by AIP Publishing. (C) Transmission spectra for co- and cross-polarized incident waves. The inset depicts the metasurface unit cell with canonical twisted helices. Reprinted figure from [96]. Copyright (2013) by IEEE. (D) Left: A metasurface asymmetrically transmitting linearly polarized light from the opposite sides and a schematic of the experimental setup. Right: Measured transmission spectra for illuminations along the $+z$ (left plot) and $-z$ (right plot) directions. Reprinted figure from [160]. Copyright (2010) by the American Physical Society. (E) Left: Artistic illustration of a metasurface which asymmetrically transmits circularly polarized light. RCP light incident from the left side is converted into LCP, while RCP light is completely reflected when incident from the right side (for visual clarity, the incident wave from the right side is shown as oblique). Right: Measured and simulated Jones matrix of the metasurface. "L" and "R" denote LCP and RCP light. Reprinted figure from [51]. Copyright (2014) by the American Physical Society.

by dissipation loss (see the plot in Figure 8C). Moreover, the helical chiral inclusions can be planarized, which is required for simple printed-circuit-board fabrication [96]. Another rigorous approach for creating polarization rotators relies on aforementioned cascades of metallic pattern sheets [52, 143, 146]. Importantly, these cascaded metasurfaces can be easily fabricated for operation at optical frequencies.

It is worth mentioning that chiral metasurfaces have also found applications as absorbers of electromagnetic waves. Despite the fact that the presence of chirality is not a necessary condition for total absorption, it was demonstrated that the use of chiral unit cells can allow some unique properties, in particular, stronger magnetic properties and off-band invisibility of the absorbing structure [168, 169].

4.2.3 Asymmetric transmission and other functionalities

Since chiral metasurfaces allow manipulation of two orthogonal polarizations, they can be potential candidates for obtaining certain effects which to some extent resemble nonreciprocal response (although of course they cannot exhibit any truly nonreciprocal effect, like isolation). Let us consider a metasurface described by the following transmission matrix:

$$\overline{\overline{S}}_{21} = e^{j\vartheta}\begin{pmatrix} 0 & 0 \\ 1 & 0 \end{pmatrix}. \tag{12}$$

Excited by x-polarized fields from the two opposite sides, it transmits incident energy into the y-polarization with different efficiencies (determined by $\overline{\overline{S}}_{21}$ and $\overline{\overline{S}}_{12} = \overline{\overline{S}}_{21}^{T}$). Such functionality, referred as "asymmetric transmission", however, does not violate reciprocity.

Observation 3. *Chirality is not a required condition for realizing a metasurface exhibiting asymmetric transmission for linearly polarized waves. However, the metasurface must be anisotropic in its plane (assuming reciprocal response).* Since 2010 there has been a number of works reporting on such metasurfaces [143, 160, 170–175]. Figure 8D illustrates one of the designed metasurfaces formed by two layers of metallic patterns. As can be seen from the right panel of the figure, the cross-polarization transmission coefficient t_{yx} equals 0 or 0.3 depending on the illumination direction.

Likewise, asymmetric transmission can be realized for circularly polarized waves. In this case, when RCP light

is incident on a metasurface from one side, it is fully transmitted with polarization changed to LCP. At the same time, when incident from the opposite side, RCP light is completely reflected back with the same polarization. Thus, conversion of the polarization in transmission becomes asymmetric: T_{LR} for illumination from side 1 is not equal to T_{LR} from side 2. The latter, due to reciprocity of the metasurface, is equivalent to T_{RL} from side 1. Thus, in the alternative formulation, the asymmetric transmission occurs when transmission coefficients T_{LR} and T_{RL} for illumination from one side are not equal. The corresponding Jones matrix of a metasurface with this response reads

$$\overline{\overline{S}}_{21} = \frac{e^{j\vartheta}}{2}\begin{pmatrix} 1 & j \\ j & -1 \end{pmatrix}. \tag{13}$$

Observation 4. *Asymmetric transmission for circularly polarized waves can be achieved in metasurfaces lacking chirality. The metasurface must be anisotropic in the plane (assuming reciprocal response)* [96, 143, 170]. Since chirality is not required in the metasurface, asymmetric transmission effect can occur in planar anisotropic or pseudochiral structures even at normal incidence [76, 176]. Recently, cascade metasurface with improved performance were synthesized based on a rigorous approach [51, 54, 143]. Figure 8E illustrates such a metasurface designed for near infrared radiation. As is seen from the plot, the metasurface provides high transmission asymmetry: $T_{LR} = 0.55$ and $T_{RL} = 0.03$ at the operating frequency. Another approach for designing asymmetric transmission response was proposed based on metallic helices that change their handedness halfway along the helix axis [56].

There are other functionalities available with chiral metasurfaces; however, in most of them, chirality is not a required property for them and plays a secondary role. In particular, rotation of polarization in reflection regime is easily available with anisotropic metasurfaces backed with a ground plane [177–179] (note that the rotation directions are different for vertical and for horizontal linear polarizations of incident waves due to reciprocity). However, by introducing chirality in the metasurface, one can enable some additional exotic features such as off-band transparency [57, 75]. Recently, an interesting application of chiral metasurfaces for controlling optical forces was suggested [180].

4.3 Asymmetric reflection

As it was shown above, chiral metasurfaces have great potential in applications for various polarization transformers. In contrast, omega metasurfaces do not change polarization of incident waves, however, they offer another functionality which is inaccessible with usual anisotropic structures: asymmetric co-polarized (without change of polarization) reflection for waves normally incident on the metasurface from the opposite directions.

Let us consider an omega metasurface made of basic Ω-shaped inclusions as shown in Figure 9A. In the first scenario, it is illuminated by a plane wave with the *x*-oriented electric field $\mathbf{E}_i$ propagating along the +*z*-direction. In the second scenario, the direction of the incidence is reversed (see Figure 9B). According to (9), due to the orientation of the incident fields $\mathbf{E}_i$ and $\mathbf{H}_i$, all the polarizability components contribute to the induced dipole moments **p** and **m**. Here, for simplicity of the analysis, we consider

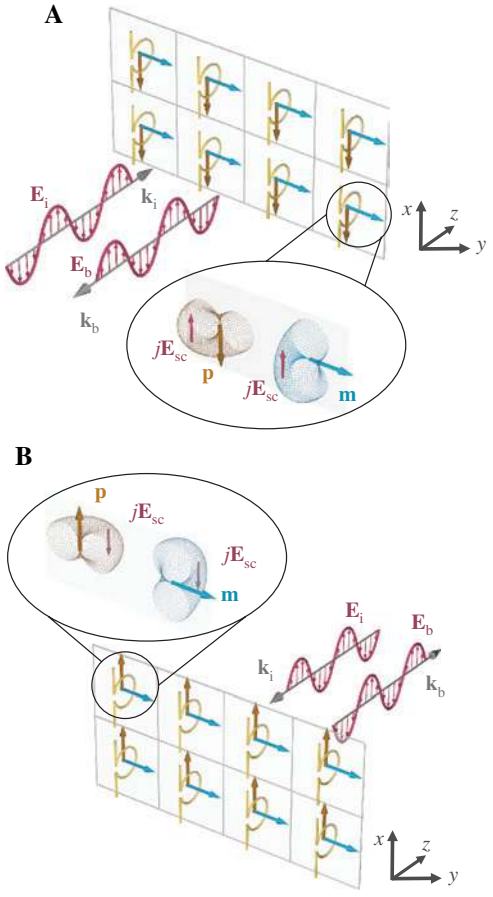

Figure 9: Illustration of asymmetric co-polarized reflection enabled by omega bianisotropic coupling in the metasurface. Illumination is along (A) the +*z* and (B) –*z* direction. For clarity, only dipole moments generated due to bianisotropic coupling are shown: $\mathbf{p} = \overline{\overline{\tilde{\alpha}}}_{em} \cdot \mathbf{H}_i$ and $\mathbf{m} = \overline{\overline{\tilde{\alpha}}}_{me} \cdot \mathbf{E}_i$. The insets depict the radiation patterns of the dipole moments. Only one half of each pattern is shown. Total backscattered (reflected) field from the metasurface is different for different illuminations.

only those parts of the dipole moments which are created due to bianisotropic polarizabilities, i.e. $\mathbf{p}=\bar{\bar{\hat{\alpha}}}_{\mathrm{em}}\cdot\mathbf{H}_{\mathrm{i}}$ and $\mathbf{m}=\bar{\bar{\hat{\alpha}}}_{\mathrm{me}}\cdot\mathbf{E}_{\mathrm{i}}$. It can be proven that the other dipole contributions due to polarizabilities $\bar{\bar{\hat{\alpha}}}_{\mathrm{ee}}$ and $\bar{\bar{\hat{\alpha}}}_{\mathrm{mm}}$ always generate the same reflected waves regardless of the illumination direction (as in the case of a simple layer of an isotropic magnetodielectric). Figure 10A shows the orientations of the induced dipole moments in the metasurface due to bianisotropic coupling for the two scenarios ($\hat{\alpha}_{\mathrm{em}}$ and $\hat{\alpha}_{\mathrm{me}}$ were assumed to be real valued). The dipole moments radiate plane waves with the same linear polarizations (see the radiation patterns in the insets; for clarity, only one half of each radiation pattern is shown). The backscattered fields $\mathbf{E}_{\mathrm{b}}$ for both scenarios can be determined using (7) and (8). Comparing Figure 9A and B, it is seen that the backscattered field has the opposite signs in the two scenarios: $j\mathbf{E}_{\mathrm{sc}}$ and $-j\mathbf{E}_{\mathrm{sc}}$. This results in the asymmetry of the total reflected field (created by the total dipole moments) when the metasurface is illuminated from the $-z$- and $+z$-directions.

Observation 5. *Asymmetric co-polarized reflection (amplitude and/or phase) from a reciprocal metasurface normally illuminated from its opposite sides requires bianisotropic omega coupling* [181]. As it was mentioned in Section 4.1, simple examples of planar structures possessing asymmetric reflection are high-impedance surfaces. One of their sides is a ground plane (with zero impedance); therefore, the reflection coefficient for waves incident on this side is –1. While the surface impedance of the other side is engineered to be infinite (e.g. by corrugating the surface [183, 184] or by introducing so-called mushroom-type patch array structure [130]), resulting in the +1 reflection coefficient for waves impinging on this side. Figure 10A depicts a mushroom-type high-impedance surface. The upper metallic layer with the "mushroom" shape provides required impedance.

Such high-impedance surfaces can be described in terms of bianisotropic omega coupling. An alternative realization of asymmetric reflection based on an array of subwavelength omega inclusions was suggested in [181]. The absence of a ground plane in the design makes the structure transparent at frequencies outside the resonance [63, 185]. The asymmetry of reflection occurs due to asymmetric shape of the metallic omega inclusion shown in Figure 10B (note that this inclusion is equivalent to that depicted in Figure 2B but has opposite sign of magnetoelectric coupling). As is seen from Figure 10B, the omega metasurface reflects with the same amplitude but different phases when illuminated from the opposite sides. Subsequently, the idea of ground-plane-free metasurfaces for asymmetric reflection was pushed toward optical frequencies using plasmonic [64, 186] and dielectric [66] inclusions. As it was demonstrated in [182, 187], asymmetric co-polarized reflection response can be achieved in metasurfaces with symmetric inclusions if it is deposited onto substrate (or superstrate) with enough high dielectric permittivity (see Figure 10C). Such effect was named "substrate-induced bianisotropy".

Enabling dissipation loss in the metasurface, one can design asymmetric absorbers for normal incidence which provide different amplitudes of reflection coefficient from different sides [64, 65, 131, 188, 189]. Figure 10D illustrates a metasurface with asymmetric gold inclusions, which can be tuned to absorb different amount of impinging energy from different directions in the near infrared.

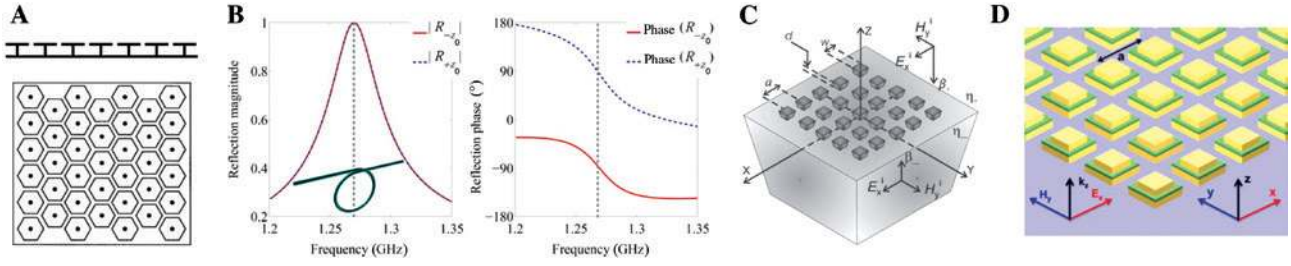

Figure 10: Metasurfaces for asymmetric co-polarized reflection.
(A) Side and top views of a mushroom-type high-impedance surface possessing bianisotropic omega response. Reprinted figure from [130]. Copyright (1999) by IEEE. (B) The amplitudes (left) and phases (right) of co-polarized reflection coefficient for opposite illumination directions of an omega metasurface. Due to the absence of a ground plane, the reflection coefficient reaches unit only at the resonance. The inset shows the metasurface unit cell with a metallic omega inclusion. Reprinted figure from [181]. Copyright (2014) by IEEE. (C) A planar array of plasmonic inclusions at the interface between two different media with characteristic impedances η_+ and η_-. Due to the contrast of the impedances omega bianisotropic effects are induced in the metasurface with symmetric inclusions. Reprinted figure from [182]. Copyright (2015) by the American Physical Society. (D) Geometry of a plasmonic omega metasurface for asymmetric absorption of normally incident waves in the near infrared. Reprinted figure from [64]. Copyright (2015) by the American Physical Society.

The aforementioned results in this section correspond to the case of asymmetric reflection without polarization transformations (reflected and incident waves have the same polarization). However, if such transformations occur, asymmetric reflection can be achieved even without omega bianisotropic coupling.

Observation 6. *Asymmetric cross-polarized reflection from a metasurface normally illuminated from its opposite sides can be achieved only if it possesses anisotropic (in the plane) electric or/and magnetic responses. Bianisotropic properties are not required.* Asymmetric cross-polarized reflection occurs, for example, in metasurfaces considered in Section 4.2.3.

4.4 Non-reciprocal bianisotropic effects

Nonreciprocal response in planar structures is essential for realizing various types of isolators which pass electromagnetic radiation along one direction and block it along the opposite direction, as well as other nonreciprocal devices. Nonreciprocal metasurfaces without bianisotropy can be realized as two-dimensional arrays of small inclusions whose electric $\overline{\overline{\alpha}}_{ee}$ or/and magnetic $\overline{\overline{\alpha}}_{mm}$ polarizability dyadics possess nonzero antisymmetric parts. A typical example is an array of small magnetized ferrite spheres. Field interactions between resonant nonreciprocal spheres leads to very wide frequency bands of the resonant response of the metasurface, as compared with the response of one inclusion and of solid slabs of the same material [190]. Alternative realization of nonreciprocal response in metasurfaces is based on the use of active circuits which are embedded in meta-atoms [191, 192]. One of such metasurfaces is shown in Figure 11A. Due to proper tuning of the circuit with an electronic amplifier, Faraday-like rotation effect was achieved for radiation passing through the metasurface: polarization plane of linearly polarized waves, impinging on the metasurface from different sides, is rotated in the opposite directions. Another example is an anisotropic nonreciprocal metasurface proposed in [192] which unidirectionally (only alone one direction) transmits circularly polarized light. There are other possible means to break time-reversal symmetry of metasurface response and enable nonreciprocal effects, including nonreciprocal bianisotropic coupling. In particular, we would like to mention time modulation of meta-atom properties and the use of nonlinear effects.

Observation 7. *The Faraday rotation effect (nonreciprocal circular birefringence) does not require bianisotropic response in the metasurface. Similarly, circular polarization isolators can be built based on anisotropic nonreciprocal surfaces.*

Enabling bianisotropic coupling dramatically extends the range of functionalities achievable with nonreciprocal metasurfaces. A metasurface with Tellegen bianisotropic coupling (see its individual inclusion in Figure 4A) provides additional control over cross-polarized reflected fields. The authors of [195] demonstrated that a thin uniaxial layer of Tellegen composite (effectively, a metasurface) provides the effect of reflection in cross-polarization for arbitrary polarization of linearly polarized incident waves. Note that in this case the polarization plane of the reflected wave

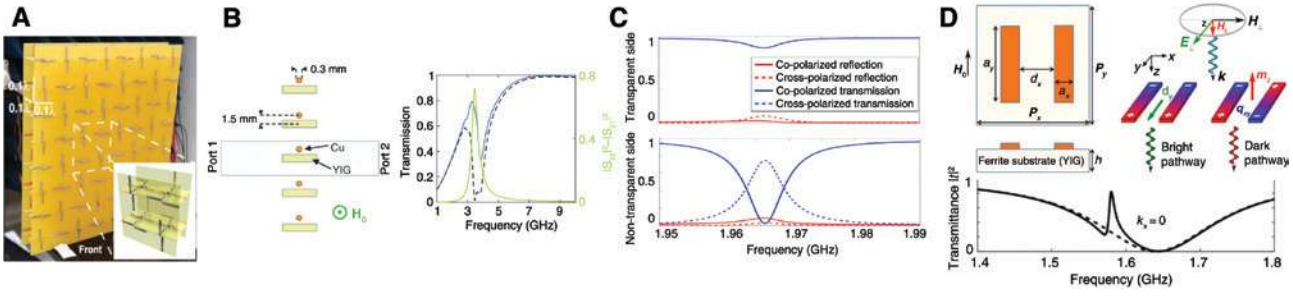

Figure 11: Metasurfaces exhibiting nonreciprocal anisotropic and bianisotropic effects.
(A) A photo of anisotropic magnet-less metasurface exhibiting the Faraday rotation. Reprinted figure from [191]. Copyright (2012) by United States National Academy of Sciences. (B) Left: Schematic of nonreciprocal metasurface with pure artificial moving coupling. Right: Transmission spectra when the structure is illuminated from the left ($|S_{21}|^2$, dashed black curve) and from the right ($|S_{12}|^2$, blue curve). Reprinted figure from [193]. Copyright (2014) by the American Physical Society. (C) Simulated reflectance and transmittance spectra for a metasurface with ferrite inclusions shown in Figure 4B. The top and bottom plots correspond to the two opposite illumination directions. Reprinted figure from [101]. Copyright (2014) by the American Physical Society. (D) Top: Geometry of a bianisotropic metasurface exhibiting the effect of gyromagnetically induced transparency. Bottom: Transmittance spectra for the "bright" (dashed line; $H_0 = 0$) and "dark" (solid line; $H_0 \neq 0$) modes. Reprinted figure from [194]. Copyright (2014) by the American Physical Society.

rotates always in the same direction, violating reciprocity. For example, the $+x$-oriented incident field is reflected as the $+y$-oriented field. However, when one "reverses" the time flow so that the incident field is $+y$-oriented, the reflected field will be oriented along the $-x$, contradicting to the previously considered state. Such response is nonreciprocal and is opposite to the similar reciprocal effect considered in the last paragraph of Section 4.2.3.

Observation 8. *Nonreciprocal effect of polarization rotation in reflection for incident waves with arbitrary polarization can occur only in uniaxial metasurfaces with Tellegen bianisotropic coupling* [101]. *Moreover, Tellegen coupling can provide additional control over cross-polarized transmission, however, uniaxial response is not possible in this case.*

Interesting functionalities are available with nonreciprocal metasurfaces possessing artificial moving response (see individual inclusion in Figure 4B). Analogously to omega metasurfaces, they appear asymmetric for different illumination directions, however, in this case, the asymmetry occurs in co-polarized transmission. This effect is, obviously, of nonreciprocal nature and can find important applications for compact isolators.

Observation 9. *Asymmetric co-polarized transmission (amplitude and/or phase) through a metasurface normally illuminated from its opposite sides requires bianisotropic artificial moving coupling* [101]. The first metasurface with pure artificial moving coupling was proposed in [193]. Its unit cell comprised a bar of ferromagnetic material (yttrium iron garnet) biased by external field $\mathbf{H}_0$ and a copper wire as shown in the left panel of Figure 11B. Although such geometry of the unit cell does not generally provide pure artificial moving response, the authors cleverly chose the orientation of the meta-atom and the external field bias with respect to the incident fields so that only desired bianisotropic response is pronounced. Transmission spectra for opposite illuminations are plotted in the right panel of Figure 11B. Asymmetric response near the resonance frequency is apparent. Authors of [196] experimentally demonstrated similar metasurface with artificial moving coupling using active circuits inside the meta-atoms.

Special emphasis must be given to metasurfaces possessing mixed bianisotropic properties (combination of two or several reciprocal and nonreciprocal effects). Such characteristics are inherent to the inclusions depicted in Figure 4. In particular, the uniaxial inclusion in Figure 4B at the same time possesses reciprocal chiral and nonreciprocal artificial moving properties [81, 91], and therefore, a metasurface with these inclusions will combine two functionalities: asymmetric co-polarized transmission and polarization rotation of transmitted waves [86, 101]. Figure 11C demonstrates the simulated transmission spectra for both polarization of such a metasurface.

An interesting application of bianisotropic nonreciprocal metasurfaces (with combined response) was suggested in [194]. The unit cell consisted of two identical metal strips on top of a ferrite substrate as shown in Figure 11D. Due to the geometry of the unit cell and the orientation of field bias $\mathbf{H}_0$, the induced currents in the strips constitute two different modes: "bright" mode when the currents point in the same direction and "dark" mode when the currents are oppositely oriented. The first mode results in strong electric dipole moment d_y; hence, strong reflection and low transmission thought the metasurface. Meanwhile, the second mode corresponds to an induced magnetic moment m_z which does not radiate in the normal direction, and therefore, the metasurface becomes transparent. By dynamically tuning the amplitude of the magnetic field bias, one can selectively excite the desired mode. This functionality leads to the so-called gyromagnetically induced transparency. The bottom panel of Figure 11D shows the transmittance through the metasurface in the "bright" (dashed line) and "dark" (solid line) modes.

Interestingly, one can observe a kind of complementarity and resemblance of the effects due to reciprocal and nonreciprocal bianisotropic couplings in metasurfaces. Figure 12 illustrates this observation and summarizes the

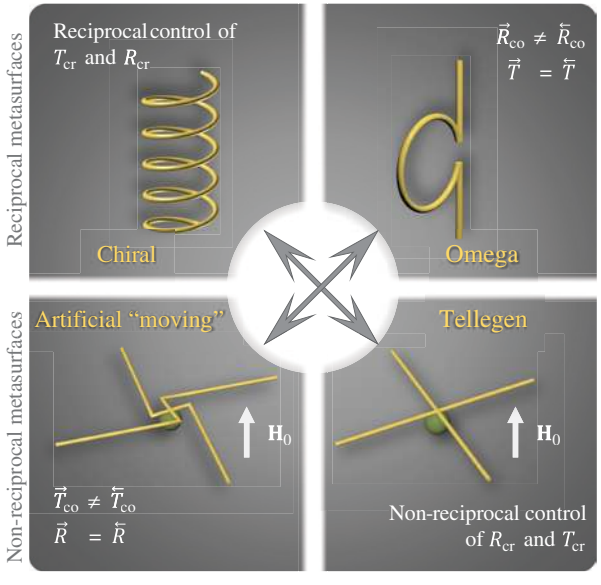

Figure 12: Illustration of functionalities enabled by uniform bianisotropic metasurfaces of four different classes. The arrows above the reflection R and transmission T coefficients indicate different directions of illumination.

characteristic functionalities achievable with bianisotropic metasurfaces of four basic classes.

Metasurfaces with Tellegen coupling enable nonreciprocal polarization transformations in reflection and transmission, while the artificial moving metasurfaces have pronounced asymmetry in transmission. In the reciprocal counterpart, chiral metasurfaces provide reciprocal polarization transformation effects, while the omega coupling makes asymmetric reflection possible. If one would be able to control all the coupling parameters in a metasurface, it would be possible to tune both reflection and transmission responses for two opposite illuminations. Allowing active response of the metasurface would further extend opportunities for electromagnetic wave control.

5 Gradient bianisotropic metasurfaces

The metasurfaces considered above are uniform, and therefore, are intended to modify only the amplitudes and phases of the reflected and transmitted plane waves. Nonuniform metasurfaces, i.e. those comprising more than one different unit cell, enable an additional functionality: wavefront manipulations. This effect is achieved via modulation of the phase and amplitude of the transmission/reflection coefficient over the metasurface plane. As a result, the direction of wave propagation as well as the wavefront shape can be modified with such gradient metasurfaces. In general, the method to design nonuniform metasurfaces is based on the local approximation where the continuous phase gradient is discretized into elements, or unit cells, which are individually designed. Each unit cell is characterized under periodic conditions (as a locally homogeneous array). Due to the subwavelength periodicity of this array, the homogenized parameters can be extracted from the scattering matrix. However, this method is accurate only if coupling differences between identical and different adjacent cells are negligible [197].

5.1 Anomalous refraction

Anomalous refraction is a basic but fundamental example of wavefront manipulation where the direction of an impinging plane wave is arbitrarily changed when it is refracted into another plane wave. Figure 13A shows an illustration of the problem where θ_i and θ_t represent the incident and refracted angles. Conventional solutions for such diffraction-based devices are optical gratings where the amount of power sent into a specific diffraction mode can be controlled [198] and transmitarray antennas, also called array lenses, which control the phase shifts introduced along the surface in the patches [199, 200]. Despite that these solutions have been extensively used, they have intrinsic drawbacks which can limit their applicability in some scenarios. In particular, diffraction gratings are effective only if reflections into only one or two propagating Floquet modes need to be canceled. Moreover, traditional devices for wave transformations are in most cases either bulky (e.g. microwave and terahertz gratings as well as optical gratings for applications in nanophotonics) or require active elements (transmitarray antennas). Below we will discuss limitations of transmitarray antennas and conventional phase-gradient metasurfaces and show that bianisotropy is necessary to eliminate parasitic reflections.

Due to their reduced thickness and ability to tailor the electromagnetic response at the subwavelength scale and for arbitrary polarizations, metasurfaces have been studied as an alternative approach for anomalous refraction. The first design method for a metasurface capable of modifying the wavefront in transmission was based on the same principle as that of conventional transmitarrays, i.e. the implementation of a linear phase shift profile along the metasurface which provides an additional tangential momentum, modifying the direction of the refracted wave [201, 202]. Such metasurfaces were called gradient referring to the phase gradient along the surface which is defined as $\Phi(x) = k_1 \sin\theta_i x - k_2 \sin\theta_t x$ (k_1 and k_2 are the wavevectors in the two media surrounding the metasurface, x is the coordinate along the direction of phase gradient).

A well-known approach for the design of refractive gradient metasurfaces is based on the use of Huygens' meta-atoms [13, 123, 203]. The Huygens meta-atoms with balanced electric and magnetic responses provide full transmission and phase control. Although the initially proposed Huygens' meta-atoms were nonbianisotropic, it was soon realized that bianisotropic effects can provide additional degrees of freedom in device design. Most of the known Huygens' meta-atoms cancel reflections only at the design frequency, casting shadows at other frequencies. However, this property limits the implementation of multifunctional engineered materials that possess different functionalities at different frequencies by cascading metasurfaces. For the design of off-band invisible meta-atoms, one can tailor the electric and magnetic dipole

response in such a way that they are always balanced in the range of frequencies of interest. This regime can be achieved using two different approaches: by spectrally overlapping the electric and magnetic dipole resonances in multimode low-loss inclusions [204–206] or by exciting the same resonant mode in single-wire bianisotropic meta-atoms [169, 207] which ensures broadband reflection cancellation.

As it was demonstrated in [207], the design of non-reflecting particles which are transparent at other frequencies can be obtained with uniaxial chiral elements. However, meta-atoms based on single-wire chiral inclusions create cross-polarized fields and are not fully suitable for the design of gradient metasurfaces which should not change the wave polarization. For this reason, the authors proposed an alternative approach where each unit cell consists of more than one bianisotropic inclusion, and the total chirality is compensated. Figure 13B shows the geometry of the metasurface with inclusions of the opposite handedness. The scattering properties of the metasurface designed for refracting normally incident waves at 45° from the normal (see Figure 13B) shows that the reflection is nearly zero in a very broad frequency range.

Recent studies have shown that anomalous refraction devices based on anisotropic surfaces do not ensure the desired performance (especially for high contrast between the incident and refracted angles) and some part of the energy is spread into other directions [13, 126, 210]. In other words, the efficiency of phase-gradient metasurfaces, defined as the ratio of power refracted into the desired direction and that of the incident wave, is reduced due to existence of parasitic reflections. The theoretical limit for the efficiency of anisotropic gradient metasurfaces was derived in [13] and is plotted in Figure 13C (the case of normal incidence is considered). As is seen, the achievable efficiency of such metasurfaces decreases dramatically for large refraction angles. The reduction in the efficiency is due to the wave impedance mismatch of the incident and refracted waves. This mismatch can be eliminated using surfaces with asymmetric input impedance seen at the opposite sides, i.e. bianisotropic omega metasurfaces. Indeed, think of an ideal gradient metasurface which transmits all normally incident energy from side 1 into a single diffracted mode at 45° from the normal on side 2 (producing zero reflection). If such a metasurface is illuminated normally from side 2, the incident wave is

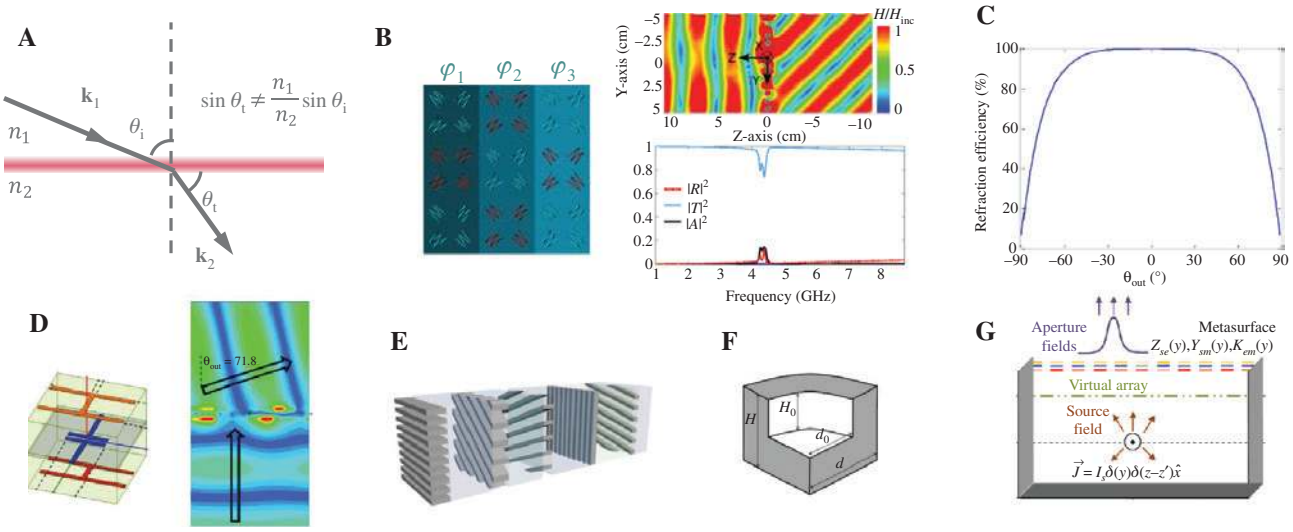

Figure 13: Wavefront manipulation of refracted waves by bianisotropic metasurfaces.
(A) Illustrative representation of the anomalous refraction scenario. (B) Huygens' metasurfaces with controlled bianisotropic response: gradient metasurface for anomalous refraction based on single-wire chiral elements. Since both electric and magnetic dipoles are excited by the same current mode, the metasurface is matched to free space in a very wide frequency range and does not produce reflections. Reprinted figure from [207]. Copyright (2016) by IEEE. (C) Efficiency of linear phase gradient metasurfaces for normal illumination as a function of the refraction angle. Reprinted figure from [13]. Copyright (2016) by the Optical Society of America. (D) Left: Bianisotropic omega inclusion made of three impedance layers as a unit cell of metasurface for perfect anomalous refraction from 0° to 80°. Right: Electric field distribution from the metasurface. Reprinted figure from [208]. Copyright (2017) by IEEE. (E) Unit cell composed of a stack of silicon gratings with different crystal axes orientations. Reprinted figure from [54]. Copyright (2017) by IEEE. (F) Unit cell composed of a dielectric asymmetric nanocylinder (one quarter of the nanocylinder is shown). Reprinted figure from [67]. Copyright (2016) by the Optical Society of America. (G) Conceptual illustration of a low-profile single-feed cavity-excited bianisotropic metasurface antenna, capable of generating an arbitrary desirable field distribution on its aperture. Reprinted figure from [209]. Copyright (2017) by IEEE.

partially reflected back in side 2, because it is actually matched for the incidence from the 45° direction. Thus, the co-polarized reflection coefficient for normal incidence is different for illuminations of the opposite sides, which corresponds to the bianisotropic omega response, as is shown in Figure 9.

Observation 10. *For the design of perfect-refraction gradient metasurfaces, one must ensure both phase and impedance matching between the incident and refracted waves, and fulfilling these conditions requires omega-type bianisotropy* [126, 210, 211]. This finding has opened a new research direction on bianisotropic gradient metasurfaces with fully controllable bianisotropic response of the meta-atoms. Although the local approach used for designing Huygens' gradient metasurfaces is also applicable in this scenario, the design conditions are more complicated and both transmission and reflection have to be tailored for both forward and backward illuminations.

First, systematic engineering of a bianisotropic gradient metasurface was proposed based on a cascade of three electrically polarizable sheets [210]. In this scenario, the value of the surface admittance of each sheet is uniquely defined by the desired bianisotropic response. For microwaves, each admittance sheet can be implemented by patterning a conductive layer on a conventional printed circuit board [208, 212]. Figure 13D illustrates geometry of a single bianistropic inclusion of the fabricated metasurface [208]. The right panel depicts the simulated electric field distribution generated by the metasurface that was designed for refracting normally incident plane waves at angle 71.8°. The experimental results confirmed that omega gradient metasurfaces can provide refraction efficiencies greatly exceeding the theoretical limit in Figure 13C.

In the optical domain, where the use of metals is limited by high ohmic losses, all-dielectric meta-atoms with bianisotropic response are potential candidates for improving the performance of gradient metasurfaces. For example, a dielectric unit cell composed of a stack of different dielectric gratings separated by dielectric spacers (see Figure 13E) can potentially provide the desired response [54]. One can control both bianisotropic couplings in the metasurface: omega coupling via the asymmetry between the layers and the chiral coupling via the mutual twist of the dielectric layers. However, this solution can present important drawbacks for the design of gradient metasurfaces due to the considerable thickness of the structure and strong interactions between adjacent unit cells, which limits the use of the local approach in the design and forces the use of numerical optimizations for controlling the near fields. More compact topologies, like asymmetric dielectric nanocylinders [67] (see Figure 13F), may provide better performance within the local design approach.

Bianisotropic gradient metasurfaces can be used also in other applications. By controlling the evanescent fields at both sides of the metasurface a perfect reflectionless wide-angle beam splitter can be designed [211]. Another application is the design of low-profile antennas, where a gradient bianisotropic metasurface can control the aperture field distribution of a single-feed cavity [209] (see the example shown in Figure 13G). In general, the control over transmission and reflection amplitudes and phases offered by bianisotropic meta-atoms opens new possibilities for the design of more complex devices for wavefront manipulations such as lenses and holograms.

5.2 Anomalous reflection

Metasurfaces have been also used for controlling reflected wavefronts. In analogy to the refractive case, a wave is anomalously reflected if it does not follow the classical reflection law, meaning that the angle of reflection, θ_r, is not equal to the incidence angle, θ_i, as shown in Figure 14A. Most metasurfaces for reflection engineering are realized as some reciprocal composite layers backed by a continuous metal screen. Obviously, the reflection properties of such thin layers are different for illuminations from the side of the composite layer and the side of the metal plate. Thus, these metasurfaces are omega-type bianisotropic layers, and the magnetoelectric coupling phenomena are essential for the operation of anomalous reflectors.

The simplest method for approaching the problem of anomalous reflection is following the generalized reflection law [201] (also recognized as the phased-array antenna principle). In this case, using the local design methodology, the elements of the array can be designed for producing a linear variation of the phase shift in reflection according to $\Phi(x) = k_1(\sin\theta_i - \sin\theta_r)x$ (note that the local design approach assumes only gradient of the phase, while amplitude of reflection is fixed and equal to unity). The 2π-phase gradient in reflection requires control of both electric and magnetic responses and it is typically obtained by using grounded metasurfaces [214, 215]. In this case, the reflection amplitude can be very high if low-loss materials are used. The presence of a metal ground plane forbids transmission at all frequencies that makes the metasurface impenetrable.

An alternative solution can be found with the use of nongrounded arrays of bianisotropic scatterers that

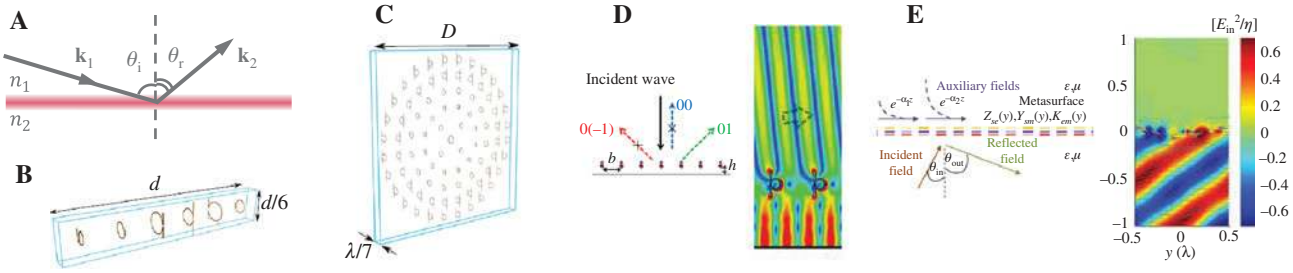

Figure 14: Wavefront manipulations of reflected waves by gradient bianisotropic metasurfaces.
(A) Schematic representation of the anomalous reflection scenario, where θ_i and θ_r represent the incidence and reflection angles. The metasurface is shown in red. (B) One period of a ground-free metasurface consisting of copper inclusions that provide a linear phase variation of the reflection spanning a 2π range. Reprinted figure from [63]. Copyright (2015) by the American Physical Society. (C) A nonperiodic metasurface composed of 6 concentric arrays of omega inclusions and designed for focusing incident waves in reflection. Reprinted figure from [63]. Copyright (2015) by the American Physical Society. (D) Meta-grating for perfect anomalous reflection based on bianisotropic omega inclusions and corresponding electric field distribution of the scattered waves. Reprinted figure from [213]. Copyright (2017) by the American Physical Society. (E) Simulated reflected electric field distribution from a bianisotropic gradient metasurface. Perfect anomalous reflection is accomplished based on the excitation of auxiliary evanescent fields. Reprinted figure from [211]. Copyright (2016) by the American Physical Society.

allow re-radiation of waves in the backward direction with different phases, while in the forward direction, they scatter waves with the same phase, opposite to that of the incident plane wave. Due to the absence of the ground plane, the metasurface appears nearly absolutely transparent at frequencies outside the resonance band (off-band transparency). As shown in [63, 181], the scattered field in the backward direction is proportional to $\mathbf{E}_{\text{back}} \propto (\overline{\overline{\hat{\alpha}}}_{\text{ee}} + 2\overline{\overline{\hat{\alpha}}}_{\text{me}} - \overline{\overline{\hat{\alpha}}}_{\text{mm}})$, while the scattered field into the forward direction is proportional to $\mathbf{E}_{\text{forward}} \propto (\overline{\overline{\hat{\alpha}}}_{\text{ee}} + \overline{\overline{\hat{\alpha}}}_{\text{mm}})$. Thus, the magnetoelectric polarizability, $\overline{\overline{\hat{\alpha}}}_{\text{me}}$, enables additional freedom in the metasurface design and can be used for the realization of independent control of scattering in the backward and forward directions using only a single-layer array of small resonant inclusions. Figure 14B shows a schematic of a bianisotropic anomalous reflector consisting of different omega inclusions.

Another example of bianisotropic gradient metasurface is a focusing lens operating in reflection regime. Figure 14C illustrates a single-layer ground-free metasurface composed of concentric arrays of subwavelength bianisotropic inclusions. The local phase profile is parabolic in this case: $\Phi(r) = \phi_0 + \omega / c\sqrt{r^2 + f^2}$, where f is the focal distance and r is the radius of the corresponding concentric array. It should be noted that this metalens possesses asymmetrical focusing properties with respect to the propagation direction of incident waves, which is a common feature of omega layers.

It has been recently demonstrated that phase-gradient (the amplitude is constant) design scheme used for the above mentioned both impenetrable and off-band transparent metasurfaces is not accurate and its efficiency is fundamentally limited [126, 216–218]. The local design of lossless phase-gradient metasurfaces for perfect anomalous reflection requires that the normal component of the Poynting vector vanishes at the metasurface, a feature only satisfied for retro-reflection or specular reflection scenarios [219]. In the most general case, the incident and anomalously reflected plane waves interfere, generating modulation of the power flow which does not allow us to satisfy the condition of zero power flow into lossless boundaries using flat surfaces without exciting some additional, evanescent waves close to the metasurface. As a consequence of the imprecise design process, part of the incident energy is scattered into undesired directions reducing the efficiency of the metasurface. The efficiency limit of anomalously refracting and reflecting metasurfaces based on a linear phase gradient follow the same curve (see Figure 13C). For small reflection angles (up to 60°), the required reflection phase variations are slow and the conventional simple phase-gradient design approach works quite well. However, for wider reflection angles, the efficiency drops dramatically [216, 218].

For a limited range of relations between the incidence and reflection angles, when the required period of the metasurface is such that not more than three propagating Floquet modes exist, reflections into the unwanted modes can be cancelled using diffraction gratings. Often, it is enough to position only one or two scatters in each period of the array to nearly perfectly cancel reflections into the unwanted directions (first of all, specular reflection). Such devices are called blazed gratings or binary gratings [220]. Recently, a realization of this approach with the use of bianisotropic omega scatterers has been theoretically proposed [213]. Figure 14D shows a schematic representation of the operation principle and the reflected field

distribution from a meta-grating designed for reflecting the normally incident energy into 83°.

Another theoretical proposal for fulfilling the condition of zero normal component of the Poynting vector at the reflecting boundary is based on excitation of auxiliary evanescent fields propagating along the interface [211]. Figure 14E shows simulated field distribution of scattered waves from a metasurface designed by this approach. In this particular case, two evanescent waves are carefully designed for mimicking the normal component of the Poynting vector produced by the propagating waves at the other side of the metasurface. One can see the field distribution at both sides of the metasurface and power flow marked with gray lines.

The actual design of 100% efficient metasurfaces exhibiting anomalous reflection [211, 216, 218] is possible only if they possess strongly nonlocal response [216]. The spatial dispersion in these structures is stronger than that modeled by the omega coupling coefficient. Importantly, the requirement of strong nonlocal response can be lifted if the metasurface is designed in such a way that the anomalously reflected wave has orthogonal polarization to that of incident wave. In this case, there is no interference between the incident and reflected waves and the metasurface can be designed locally. The transformation of polarization into an orthogonal one can be accomplished with anisotropic [221] or chiral metasurfaces [126].

6 Conclusions and discussions

In recent years, interest in bianisotropic metasurfaces has expanded to a large degree due to their capability for advanced wavefront manipulations. However, it was the studies of uniform bianisotropic metasurfaces that led the way toward understanding the means of achieving complete control of the electromagnetic response of thin layers. From these studies, we know that chiral meta-atoms, in which the induced electric (magnetic) moment and the exciting magnetic (electric) field vectors

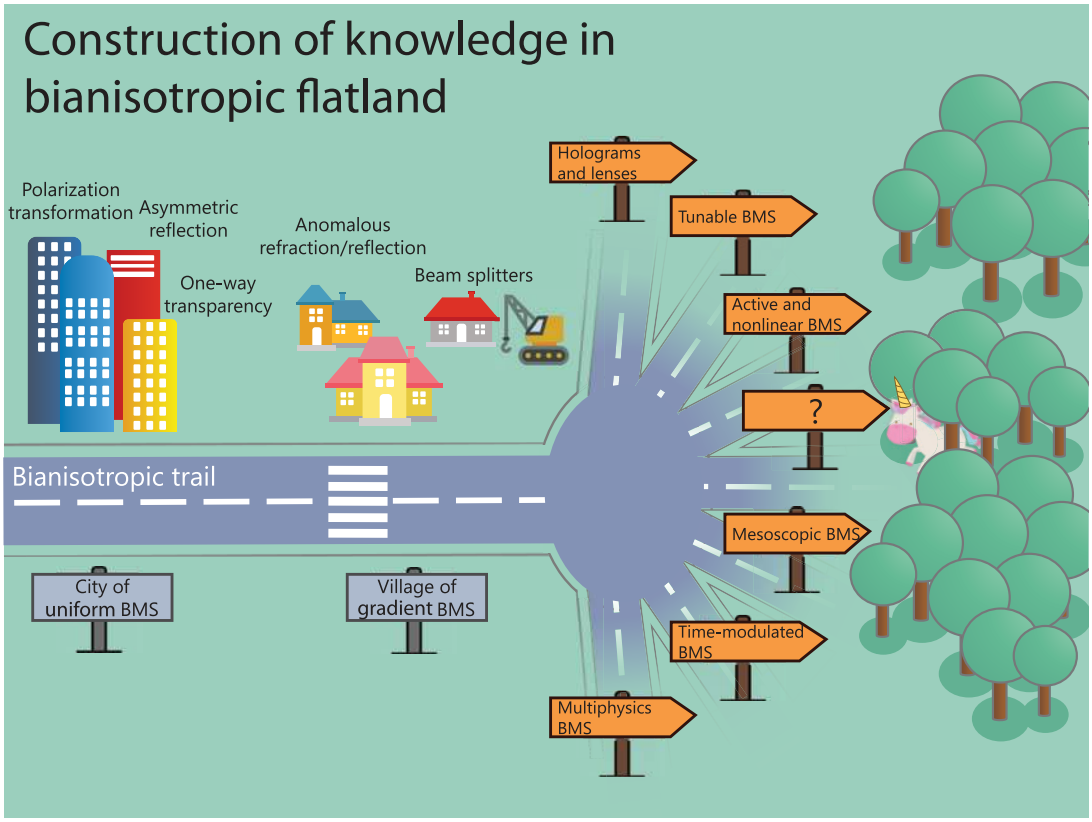

Figure 15: Illustration of the evolution of the knowledge on bianisotropic metasurfaces (BMS) and its prospective research directions. Bianisotropic flatland represents all the possible functionalities offered by the most general linear metasurfaces. In bianisotropic flatland, our knowledge is represented by man-made constructions: the complex city represents the well-studied research directions, whereas the village represents recent ideas and studies that have not been fully analyzed yet. In contrast, the mysterious forest with the unicorn symbolizes emerging but not yet explored research directions on bianisotropic metasurfaces and their applications.

are collinear, are necessary for creation of uniaxial polarization rotating metasurfaces and circular-polarization-selective metasurfaces. In contrast, omega meta-atoms, in which the induced moments and the exciting fields are orthogonal, allow realization of co-polarized asymmetric reflection. Furthermore, the two fundamental nonreciprocal types of bianisotropy have been successfully used for creating compact one-way transparent metasurfaces.

As a result of accumulated deep knowledge on uniform bianisotropic metasurfaces, we have solid foundations that allowed us to continue moving toward new goals. One of the most immediate application of bianisotropy is perfect wavefront manipulations with gradient (nonuniform) metasurfaces. It has been demonstrated that omega-type bianisotropy is a fundamental requirement for the design of 100% efficient anomalous refractive and reflective metasurfaces.

Despite all these advances, there is still a long way to go and the expectations for the application possibilities of bianisotropic metasurfaces increase. The design of more complex reciprocal metasurfaces for wavefront transformation (e.g. holograms, lenses) can benefit from the new knowledge extracted from the studies of anomalous reflection and refraction of plane waves. Only basic phenomena enabled by nonreciprocal bianisotropic metasurfaces have been explored so far. Moreover, there are rather promising directions leading to the creation of active bianisotropic metasurfaces, nonlinear bianisotropic metasurfaces, and time-modulated bianisotropic metasurfaces. Another challenge is the design of tunable, and eventually software-defined, bianisotropic metasurfaces providing different operations modes, dynamically and adaptively adjusted to the environment.

In addition, the results obtained for manipulations of electromagnetic waves can be extended and generalized for finding means to manipulate waves of different nature such as acoustic or elastic waves. Even further, one can think about metasurfaces simultaneously controlling and transforming waves of different nature, which can lead to the creation of multiphysics bianisotropic metasurfaces.

Bianisotropy is a first-order spatial dispersion effect and the structures considered in this paper are dense arrays where the sizes of the unit cells are small in comparison with the wavelength. In the case of less dense arrays (still under the diffraction limit), by exploring higher-order terms of nonlocal response function expansion, new interesting features and phenomena of wave-matter interaction could be potentially discovered. We classify this metasurface type as mesoscopic bianisotropic metasurfaces.

Figure 15 illustrates the evolution of the knowledge on bianisotropic metasurfaces and its prospective advancements. There is no doubt that new ideas and research directions will emerge, and although we cannot predict where these unpaved roads will take us, we can expect an exciting journey.

Acknowledgments: This work was supported by the Academy of Finland (projects 13287894 and 13309421) and the Nokia Foundation (201610246). The authors thank Mr. Dimitrios Tzarouchis for useful discussions about the illustration content of the last figure.

References

[1] Smith DR, Kroll N. Negative refractive index in left-handed materials. Phys Rev Lett 2000;85:2933–6.
[2] Shelby RA, Smith DR, Schultz S. Experimental verification of a negative index of refraction. Science 2001;292:77–9.
[3] Engheta N, Ziolkowski RW. Metamaterials: physics and engineering explorations. Piscataway, NJ: John Wiley & Sons, IEEE Press, 2006.
[4] Capolino F. Metamaterials handbook. Boca Raton, FL: CRC Press, 2009.
[5] Soukoulis CM, Wegener M. Past achievements and future challenges in the development of three-dimensional photonic metamaterials. Nat Photonics 2011;5:523–30.
[6] Holloway CL, Kuester EF, Gordon JA, O'Hara J, Booth J, Smith DR. An overview of the theory and applications of metasurfaces: the two-dimensional equivalents of metamaterials. IEEE Antennas Propag M 2012;54:10–35.
[7] Valev VK, Baumberg JJ, Sibilia C, Verbiest T. Chirality and chiroptical effects in plasmonic nanostructures: fundamentals, recent progress, and outlook. Adv Mater 2013;25:2517–34.
[8] Yu N, Capasso F. Flat optics with designer metasurfaces. Nat Mater 2014;13:139–50.
[9] Minovich AE, Miroshnichenko AE, Bykov AY, Murzina TV, Neshev DN, Kivshar YS, Functional and nonlinear optical metasurfaces. Laser Photonics Rev 2015;9:195–213.
[10] Tretyakov SA. Metasurfaces for general transformations of electromagnetic fields. Phil Trans R Soc A 2015;373:20140362.
[11] Glybovski SB, Tretyakov SA, Belov PA, Kivshar YS, Simovski CR. Metasurfaces: from microwaves to visible. Phys Rep 2016;634:1–72.
[12] Chen H-T, Taylor AJ, Yu N. A review of metasurfaces: physics and applications. Rep Prog Phys 2016;79:076401.
[13] Epstein A, Eleftheriades GV. Huygens' metasurfaces via the equivalence principle: design and applications. JOSA B 2016;33:A31–50.
[14] Monticone F, Alù A. Metamaterial, plasmonic and nanophotonic devices. Rep Prog Phys 2017;80:036401.
[15] Agranovich VM, Ginzburg VL. Spatial dispersion in crystal optics and the theory of excitons. New York: Interscience, 1966.
[16] Fedorov FE. Theory of gyrotropy. Minsk: Nauka i Technika, 1976.
[17] Post EJ. Formal structure of electromagnetics. Amsterdam: North-Holland Publishing Company, 1962.

[18] Mandelshtam LI. Group velocity in a crystal lattice. J Exp Theor Phys 1945;15:18.
[19] Mandelshtam LI. Lectures on some problems of the theory of oscillations (1944). In: Leontovich MA, ed. Complete collection of works, vol. 5. Moscow: Academy of Sciences, 1950: 428–67.
[20] Sivukhin DV. The energy of electromagnetic waves in dispersive media. Opt Spektrosk 1957;3:308–12.
[21] Dolin LS. To the possibility of comparison of three-dimensional electromagnetic systems with nonuniform anisotropic filling. Izv Vyssh Uchebn Zaved Radiofiz 1961;4:964–7.
[22] Pendry JB, Schurig D, Smith DR. Controlling electromagnetic fields. Science 2006;312:1780–2.
[23] Leonhardt U. Optical conformal mapping. Science 2006;312:1777–80.
[24] Schurig D, Mock JJ, Justice BJ, et al. Metamaterial electromagnetic cloak at microwave frequencies. Science 2006;314:977–80.
[25] Veselago VG. The electrodynamics of substances with simultaneously negative values of ϵ and μ. Phys Usp 1968;10:509.
[26] Pendry JB. Negative refraction makes a perfect lens. Phys Rev Lett 2000;85:3966–9.
[27] It should be noted that in some references the term is written with a dash, that is "bi-anisotropy".
[28] Marqués R, Medina F, Rafii-El-Idrissi R. Role of bianisotropy in negative permeability and left-handed metamaterials. Phys Rev B 2002;65:144440.
[29] Smith DR, Gollub J, Mock JJ, Padilla WJ, Schurig D. Calculation and measurement of bianisotropy in a split ring resonator metamaterial. J Appl Phys 2006;100:024507.
[30] Kong JA. Theorems of bianisotropic media. Proc IEEE 1972;60:1036–46.
[31] Serdyukov A, Semchenko I, Tretyakov S, Sihvola A. Electromagnetics of bi-anisotropic materials – theory and application, vol. 11. Amsterdam: Gordon and Breach Science Publishers, 2001.
[32] Lindell I, Sihvola A, Tretyakov S, Viitanen A. Electromagnetic waves in chiral and bi-isotropic media. Boston: Artech House, 1994.
[33] Tretyakov SA, Sochava AA. Eigenwaves in uniaxial chiral omega media. Microw Opt Technol Lett 1993;6:701–5.
[34] Tretyakov SA, Sochava AA. Proposed composite material for nonreflecting shields and antenna radomes. Electron Lett 1993;29:1048–9.
[35] Zhou J, Koschny T, Kafesaki M, Economou EN, Pendry JB, Soukoulis CM. Saturation of the magnetic response of split-ring resonators at optical frequencies. Phys Rev Lett 2005;95:223902.
[36] Tretyakov S. On geometrical scaling of split-ring and double-bar resonators at optical frequencies. Metamaterials 2007;1:40–3.
[37] Kodera T, Sounas DL, Caloz C. Artificial Faraday rotation using a ring metamaterial structure without static magnetic field. Appl Phys Lett 2011;99:031114.
[38] Mahmoud AM, Davoyan AR, Engheta N. All-passive nonreciprocal metastructure. Nat Commun 2015;6:8359.
[39] Tellegen BD. The gyrator, a new electric network element. Philips Res Rep 1948;3:81–101.
[40] Tretyakov SA. Nonreciprocal composite with the material relations of the transparent absorbing boundary. Microw Opt Technol Lett 1998;19:365–8.
[41] Onsager L. Reciprocal relations in irreversible processes. I. Phys Rev 1931;37:405–26.
[42] Onsager L. Reciprocal relations in irreversible processes. II. Phys Rev 1931;38:2265–79.
[43] Casimir HBG. On Onsager's principle of microscopic reversibility. Rev Mod Phys 1945;17:343–50.
[44] Landau LD, Lifshitz EM. Statistical physics, part 1 (course of theoretical physics). Oxford: Elsevier, 2013.
[45] Tretyakov S, Sihvola A, Jancewicz B. Onsager-Casimir principle and the constitutive relations of bi-anisotropic media. J Electromagnet Wave 2002;16:573–87.
[46] Jaggard DL, Mickelson AR, Papas CH. On electromagnetic waves in chiral media. Appl Phys 1979;18:211–6.
[47] Tretyakov SA, Mariotte F, Simovski CR, Kharina TG, Heliot JP. Analytical antenna model for chiral scatterers: comparison with numerical and experimental data. IEEE Trans Antennas Propag 1996;44:1006–14.
[48] Semchenko IV, Khakhomov SA, Samofalov AL. Transformation of the polarization of electromagnetic waves by helical radiators. J Commun Technol El+ 2007;52:850–5.
[49] Semchenko IV, Khakhomov SA, Samofalov AL. Optimal helix shape: equality of dielectric, magnetic, and chiral susceptibilities. Russ Phys J 2009;52:472.
[50] Decker M, Zhao R, Soukoulis CM, Linden S, Wegener M. Twisted split-ring-resonator photonic metamaterial with huge optical activity. Opt Lett 2010;35:1593–5.
[51] Pfeiffer C, Zhang C, Ray V, Guo LJ, Grbic A. High performance bianisotropic metasurfaces: asymmetric transmission of light. Phys Rev Lett 2014;113:023902.
[52] Pfeiffer C, Zhang C, Ray V, Guo LJ, Grbic A. Polarization rotation with ultra-thin bianisotropic metasurfaces. Optica 2016;3:427–32.
[53] Semchenko I. Gyrotropic properties of superlattices with magnetic structure in long-wave approximation. In: 3rd Int. Workshop on Chiral, Bi-isotropic and Bi-anisotropic Media "Chiral-94". (Périgeux, France), 1994:175–8.
[54] Ranjbar A, Grbic A. All-dielectric bianisotropic metasurfaces. In: 2017 IEEE International Symposium on Antennas and Propagation USNC/URSI National Radio Science Meeting, 2017:1719–20.
[55] Gansel JK, Thiel M, Rill MS, et al. Gold helix photonic metamaterial as broadband circular polarizer. Science 2009;325:1513–5.
[56] Kaschke J, Blume L, Wu L, et al. A helical metamaterial for broadband circular polarization conversion. Adv Opt Mater 2015;3:1411–7.
[57] Faniayeu I. Design and fabrication of functional helix-based metasurfaces. PhD thesis, Shizuoka University, Section 3.2.2, 2017.
[58] Faniayeu I, Khakhomov S, Semchenko I, Mizeikis V. Highly transparent twist polarizer metasurface. Appl Phys Lett 2017;111:111108.
[59] Banzer P, Woźniak P, Mick U, Leon ID, Boyd RW. Chiral optical response of planar and symmetric nanotrimers enabled by heteromaterial selection. Nat Commun 2016;7:13117.
[60] Ullah K, Garcia-Camara B, Habib M, et al. Chiral all-dielectric trimer nanoantenna. J Quant Spectrosc Radiat Transf 2018;208:71–7.
[61] Saadoun MMI, Engheta N. A reciprocal phase shifter using novel pseudochiral or Ω medium. Microw Opt Technol Lett 1992;5:184–8.
[62] Simovski CR, Tretyakov SA, Sochava AA, Sauviac B, Mariotte F, Kharina TG. Antenna model for conductive omega particles. J Electromagnet Wave 1997;11:1509–30.

[63] Asadchy VS, Ra'di Y, Vehmas J, Tretyakov SA. Functional metamirrors using bianisotropic elements. Phys Rev Lett 2015;114:095503.
[64] Alaee R, Albooyeh M, Yazdi M, et al. Magnetoelectric coupling in nonidentical plasmonic nanoparticles: theory and applications. Phys Rev B 2015;91:115119.
[65] Faniayeu I, Mizeikis V. Vertical split-ring resonator perfect absorber metamaterial for ir frequencies realized via femtosecond direct laser writing. Appl Phys Exp 2017;10:062001.
[66] Alaee R, Albooyeh M, Rahimzadegan A, Mirmoosa MS, Kivshar YS, Rockstuhl C. All-dielectric reciprocal bianisotropic nanoparticles. Phys Rev B 2015;92:245130.
[67] Asadchy V, Albooyeh M, Tretyakov S. Optical metamirror: all-dielectric frequency-selective mirror with fully controllable reflection phase. JOSA B 2016;33:A16–20.
[68] Sochava AA, Simovski CR, Tretyakov SA. Chiral effects and eigenwaves in bi-anisotropic omega structures. In: Priou A, Sihvola A, Tretyakov S, Vinogradov A, editors. Advances in complex electromagnetic materials, no. 28 in NATO ASI Series, Springer Netherlands, 1997:85–102.
[69] Tretyakov SA. Electromagnetic metamaterials: past, present, and future. Oxford, United Kingdom, 2015.
[70] Tretyakov SA. A personal view on the origins and developments of the metamaterial concept. J Opt 2017;19:013002.
[71] Asadchy V. Spatially dispersive metasurfaces. PhD thesis, Aalto University, 2017.
[72] In the case of lossy meta-atom, the second term in (3) is decomposed to nine dyads $\mathbf{a}_i\mathbf{a}_i$ and vector **b** in the third term decomposes to two real-valued vectors.
[73] Bunn CW. Chemical crystallography: an introduction to optical and X-ray methods. Oxford, United Kingdom: Clerendon Press, 1961.
[74] Williams R. Optical-rotatory power and linear electro-optic effect in nematic liquid crystals of *p*-azoxyanisole. J Chem Phys 1969;50:1324–32.
[75] Papakostas A, Potts A, Bagnall DM, Prosvirnin SL, Coles HJ, Zheludev NI. Optical manifestations of planar chirality. Phys Rev Lett 2003;90:107404.
[76] Fedotov VA, Mladyonov PL, Prosvirnin SL, Rogacheva AV, Chen Y, Zheludev NI. Asymmetric propagation of electromagnetic waves through a planar chiral structure. Phys Rev Lett 2006;97:167401.
[77] Plum E, Fedotov VA, Zheludev NI. Extrinsic electromagnetic chirality in metamaterials. J Opt A-Pure Appl Opt 2009;11:074009.
[78] Plum E, Liu X-X, Fedotov VA, Chen Y, Tsai DP, Zheludev NI. Metamaterials: optical activity without chirality. Phys Rev Lett 2009;102:113902.
[79] Marques R, Mesa F, Martel J, Medina F. Comparative analysis of edge- and broadside- coupled split ring resonators for metamaterial design – theory and experiments. IEEE Trans Antennas Propag 2003;51:2572–81.
[80] Mühlig S, Menzel C, Rockstuhl C, Lederer F. Multipole analysis of meta-atoms. Metamaterials 2011;5:64–73.
[81] Asadchy VS, Faniayeu IA, Ra'di Y, Tretyakov SA. Determining polarizability tensors for an arbitrary small electromagnetic scatterer. Phot Nano Fund Appl 2014;12:298–304.
[82] Liu XX, Zhao Y, Alù A. Polarizability tensor retrieval for subwavelength particles of arbitrary shape. IEEE Trans Antennas Propag 2016;64:2301–10.
[83] Alaee R, Rockstuhl C, Fernandez-Corbaton I. An electromagnetic multipole expansion beyond the long-wavelength approximation. Opt Commun 2018;407(Suppl. C):17–21.
[84] Kodera T, Sounas DL, Caloz C. Nonreciprocal magnetless CRLH leaky-wave antenna based on a ring metamaterial structure. IEEE Antennas Wirel Prop Lett 2011;10:1551–4.
[85] Vehmas J, Hrabar S, Tretyakov S. Transmission lines emulating moving media. New J Phys 2014;16:093065.
[86] Ra'di Y, Grbic A. Magnet-free nonreciprocal bianisotropic metasurfaces. Phys Rev B 2016;94:195432.
[87] Sounas DL, Alù A. Non-reciprocal photonics based on time modulation. Nat Photonics 2017;11:774–83.
[88] Kamenetskii EO. On the technology of making chiral and bianisotropic waveguides for microwave propagation. Microw Opt Technol Lett 1996;11:103–7.
[89] Tretyakov SA, Sihvola AH, Sochava AA, Simovski CR. Magnetoelectric interactions in bi-anisotropic media. J Electromagnet Wave 1998;12:481–97.
[90] Tretyakov SA, Maslovski SI, Nefedov IS, Viitanen AJ, Belov PA, Sanmartin A. Artificial Tellegen particle. Electromagnetics 2003;23:665–80.
[91] Mirmoosa M, Ra'di Y, Asadchy V, Simovski C, Tretyakov S. Polarizabilities of nonreciprocal bianisotropic particles. Phys Rev Appl 2014;1:034005.
[92] Semchenko IV, Khakhomov SA, Samofalov AL. Radiation of circularly polarized electromagnetic waves by the artificial flat lattice with two-turn helical elements. In: Proc. of the 10th International Conference on Complex Media and Metamaterials, Ghent, Belgium, 2004:236–9.
[93] Ra'di Y, Tretyakov SA. Balanced and optimal bianisotropic particles: maximizing power extracted from electromagnetic fields. New J Phys 2013;15:053008.
[94] Fernandez-Corbaton I, Fruhnert M, Rockstuhl C. Objects of maximum electromagnetic chirality. Phys Rev X 2016;6:031013.
[95] Saenz E, Semchenko I, Khakhomov S, et al. Modeling of spirals with equal dielectric, magnetic, and chiral susceptibilities. Electromagnetics 2008;28:476–93.
[96] Niemi T, Karilainen AO, Tretyakov SA. Synthesis of polarization transformers. IEEE Trans Antennas Propag 2013;61:3102–11.
[97] Guven K, Saenz E, Gonzalo R, Ozbay E, Tretyakov S. Electromagnetic cloaking with canonical spiral inclusions. New J Phys 2008;10:115037.
[98] Karilainen AO, Tretyakov SA. Isotropic chiral objects with zero backscattering. IEEE Trans Antennas Propag 2012;60:4449–52.
[99] Vehmas J, Ra'di Y, Karilainen AO, Tretyakov SA. Eliminating electromagnetic scattering from small particles. IEEE Trans Antennas Propag 2013;61:3747–56.
[100] Ra'di Y, Asadchy VS, Tretyakov SA. Total absorption of electromagnetic waves in ultimately thin layers. IEEE Trans Antennas Propag 2013;61:4606–14.
[101] Ra'di Y, Asadchy VS, Tretyakov SA. One-way transparent sheets. Phys Rev B 2014;89:075109.
[102] Sersic I, Tuambilangana C, Kampfrath T, Koenderink AF. Magnetoelectric point scattering theory for metamaterial scatterers. Phys Rev B 2011;83:245102.
[103] Sersic I, van de Haar MA, Arango FB, Koenderink AF. Ubiquity of optical activity in planar metamaterial scatterers. Phys Rev Lett 2012;108:223903.
[104] Albooyeh M, Asadchy VS, Alaee R, et al. Purely bianisotropic scatterers. Phys Rev B 2016;94:245428.

[105] Tretyakov S, Nefedov I, Sihvola A, Maslovski S, Simovski C. Waves and energy in chiral nihility. J Electromagnet Wave 2003;17:695–706.
[106] Ra'di Y, Asadchy VS, Tretyakov SA. Nihility in non-reciprocal bianisotropic media. EPJ Appl Metamat 2015;2:6.
[107] Asadchy VS, Ra'di Y, Tretyakov SA. Extreme electromagnetic properties with bianisotropic nihility. In: 2015 9th International Congress on Advanced Electromagnetic Materials in Microwaves and Optics (Metamaterials' 2015), 2015:19–21.
[108] Senior T. Combined resistive and conductive sheets. IEEE Trans Antennas Propag 1985;33:577–79.
[109] Idemen M. Straightforward derivation of boundary conditions on sheet simulating an anisotropic thin layer. Electron Lett 1988;24:663–5.
[110] Senior TB, Volakis JL. Approximate boundary conditions in electromagnetics. London, UK: The Institute of Electrical Engineers, 1995.
[111] Kuester EF, Mohamed MA, Piket-May M, Holloway CL. Averaged transition conditions for electromagnetic fields at a metafilm. IEEE Trans Antennas Propag 2003;51:2641–51.
[112] Simovski CR, Kondratjev MS, Belov PA, Tretyakov SA. Interaction effects in two-dimensional bianisotropic arrays. IEEE Trans Antennas Propag 1999;47:1429–39.
[113] Maslovski SI, Tretyakov SA. Full-wave interaction field in two-dimensional arrays of dipole scatterers. Int J Electron Commun (AEÜ) 1999;53:135–9.
[114] Tretyakov SA. On the homogenization of dense planar arrays of scatterers. Electromagnetics 1999;19:201–10.
[115] Tretyakov SA, Viitanen AJ, Maslovski SI, Saarela IE. Impedance boundary conditions for regular dense arrays of dipole scatterers. IEEE Trans Antennas Propag 2003;51:2073–8.
[116] Tretyakov S. Analytical modeling in applied electromagnetics. Boston: Artech House, 2003.
[117] Albooyeh M, Tretyakov S, Simovski C. Electromagnetic characterization of bianisotropic metasurfaces on refractive substrates: general theoretical framework. Ann Phys 2016;528:721–37.
[118] Dimitriadis AI, Kantartzis NV, Tsiboukis TD, Hafner C. Generalized non-local surface susceptibility model and Fresnel coefficients for the characterization of periodic metafilms with bianisotropic scatterers. J Comput Phys 2015;281:251–68.
[119] Dimitriadis AI, Sounas DL, Kantartzis NV, Caloz C, Tsiboukis TD. Surface susceptibility bianisotropic matrix model for periodic metasurfaces of uniaxially mono-anisotropic scatterers under oblique te-wave incidence. IEEE Trans Antennas Propag 2012;60:5753–67.
[120] Achouri K, Salem MA, Caloz C. General metasurface synthesis based on susceptibility tensors. IEEE Trans Antennas Propag 2015;63:2977–91.
[121] Zhao Y, Liu X-X, Alù A. Recent advances on optical metasurfaces. J Opt 2014;16:123001.
[122] Yatsenko VV, Maslovski SI, Tretyakov SA, Prosvirnin SL, Zouhdi S. Plane-wave reflection from double arrays of small magnetoelectric scatterers. IEEE Trans Antennas Propag 2003;51:2–11.
[123] Pfeiffer C, Grbic A. Metamaterial Huygens' surfaces: tailoring wave fronts with reflectionless sheets. Phys Rev Lett 2013;110:197401.
[124] Selvanayagam M, Eleftheriades GV. Discontinuous electromagnetic fields using orthogonal electric and magnetic currents for wavefront manipulation. Opt Exp 2013;21:14409–29.
[125] Epstein A, Eleftheriades GV. Passive lossless Huygens metasurfaces for conversion of arbitrary source field to directive radiation. IEEE Trans Antennas Propag 2014;62:5680–95.
[126] Asadchy VS, Albooyeh M, Tcvetkova SN, Díaz-Rubio A, Ra'di Y, Tretyakov SA. Perfect control of reflection and refraction using spatially dispersive metasurfaces. Phys Rev B 2016;94:075142.
[127] Roberts CM, Inampudi S, Podolskiy VA. Diffractive interface theory: nonlocal susceptibility approach to the optics of metasurfaces. Opt Exp 2015;23:2764–76.
[128] Lamb H. On the reflection and transmission of electric waves by a metallic grating. Proc London Math Soc 1898;29:523–44.
[129] Yatsenko VV, Tretyakov SA, Maslovski SI, Sochava AA. Higher order impedance boundary conditions for sparse wire grids. IEEE Trans Antennas Propag 2000;48:720–7.
[130] Sievenpiper D, Zhang L, Broas RFJ, Alexopolous NG, Yablonovitch E. High-impedance electromagnetic surfaces with a forbidden frequency band. IEEE Trans Microw Theory Techn 1999;47:2059–74.
[131] Ra'di Y, Simovski CR, Tretyakov SA. Thin perfect absorbers for electromagnetic waves: theory, design, and realizations. Phys Rev Appl 2015;3:037001.
[132] Tretyakov SA, Simovski CR. Dynamic model of artificial reactive impedance surfaces. J Electromagnet Wave 2003;17:131–45.
[133] Luukkonen O, Simovski C, Granet G, et al. Simple and accurate analytical model of planar grids and high-impedance surfaces comprising metal strips or patches. IEEE Trans Antennas Propag 2008;56:1624–32.
[134] Luukkonen O, Silveirinha MG, Yakovlev AB, Simovski CR, Nefedov IS, Tretyakov SA. Effects of spatial dispersion on reflection from mushroom-type artificial impedance surfaces. IEEE Trans Microw Theory Techn 2009;57:2692–9.
[135] Belov PA, Tretyakov SA. Resonant reflection from dipole arrays located very near to conducting planes. J Electromaget Wave 2002;16:129–43.
[136] Lagarkov A, Semenenko VN, Chistyaev VA, Ryabov DE, Tretyakov SA, Simovski CR. Resonance properties of bi-helix media at microwaves. Electromagnetics 1997;17:213–37.
[137] Yatsenko VV, Tretyakov SA, Sochava AA. Reflection of electromagnetic waves from dense arrays of thin long conductive spirals. Int J Appl Electromagn Mech 1998;9:191–200.
[138] Caveney S. Cuticle reflectivity and optical activity in scarab beetles: the role of uric acid. Proc R Soc Lond B Biol Sci 1971;178:205–25.
[139] Sharma V, Crne M, Park JO, Srinivasarao M. Structural origin of circularly polarized iridescence in jeweled beetles. Science 2009;325:449–51.
[140] Robert P. Reflector for circularly polarized waves. Mar. 1970. U.S. Classification 343/756, 343/781.00R, 343/909; International Classification H01Q19/10, H01Q19/195; Cooperative Classification H01Q19/195; European Classification H01Q19/195.
[141] Roy JE, Shafai L. Reciprocal circular-polarization-selective surface. IEEE Antennas Propag M 1996;38:18–33.
[142] Zhao Y, Belkin MA, Alù A. Twisted optical metamaterials for planarized ultrathin broadband circular polarizers. Nat Commun 2012;3:870.
[143] Pfeiffer C, Grbic A. Bianisotropic metasurfaces for optimal polarization control: analysis and synthesis. Phys Rev Appl 2014;2:044011.

[144] Morin GA. A simple circular polarization selective surface (CPSS). In: Antennas and Propagation Society International Symposium, 1990. AP-S. Merging Technologies for the 90's. Digest. 1990;1:100–03.
[145] Askarpour AN, Zhao Y, Alù A. Wave propagation in twisted metamaterials. Phys Rev B 2014;90:054305.
[146] Selvanayagam M, Eleftheriades GV. Design and measurement of tensor impedance transmitarrays for chiral polarization control. IEEE Trans Microw Theory Techn 2016;64:414–28.
[147] Kim M, Eleftheriades GV. Highly efficient all-dielectric optical tensor impedance metasurfaces for chiral polarization control. Opt Lett 2016;41:4831–4.
[148] Munk BA. Frequency selective surfaces: theory and design. New York: John Wiley and Sons, 2000.
[149] Selvanayagam M, Eleftheriades GV. Polarization control using tensor Huygens surfaces. IEEE Trans Antennas Propag 2014;62:6155–68.
[150] Singh R, Plum E, Zhang W, Zheludev NI. Highly tunable optical activity in planar achiral terahertz metamaterials. Opt Express 2010;18:13425–30.
[151] Shi JH, Zhu Z, Ma HF, Jiang WX, Cui TJ. Tunable symmetric and asymmetric resonances in an asymmetrical split-ring metamaterial. J Appl Phys 2012;112:073522.
[152] Leon ID, Horton MJ, Schulz SA, Upham J, Banzer P, Boyd RW. Strong, spectrally-tunable chirality in diffractive metasurfaces. Sci Rep 2015;5:srep13034.
[153] Amitay N, Saleh AAM. Broad-band wide-angle quasi-optical polarization rotators. IEEE Trans Antennas Propag 1983;31:73–6.
[154] Torres RP, Catedra MF. Analysis and design of a two-octave polarization rotator for microwave frequency. IEEE Trans Antennas Propag 1993;41:208–13.
[155] Cong L, Cao W, Zhang X, et al. A perfect metamaterial polarization rotator. Appl Phys Lett 2013;103:171107.
[156] Cong L, Cao W, Tian Z, Gu J, Han J, Zhang W. Manipulating polarization states of terahertz radiation using metamaterials. New J Phys 2012;14:115013.
[157] Shaltout A, Liu J, Shalaev VM, Kildishev AV. Optically active metasurface with non-chiral plasmonic nanoantennas. Nano Lett 2014;14:4426–31.
[158] Svirko Y, Zheludev N, Osipov M. Layered chiral metallic microstructures with inductive coupling. Appl Phys Lett 2001;78:498–500.
[159] Ye Y, He S. 90° polarization rotator using a bilayered chiral metamaterial with giant optical activity. Appl Phys Lett 2010;96:203501.
[160] Menzel C, Helgert C, Rockstuhl C, et al. Asymmetric transmission of linearly polarized light at optical metamaterials. Phys Rev Lett 2010;104:253902.
[161] Rogacheva AV, Fedotov VA, Schwanecke AS, Zheludev NI. Giant gyrotropy due to electromagnetic-field coupling in a bilayered chiral structure. Phys Rev Lett 2006;97:177401.
[162] Kanda N, Konishi K, Kuwata-Gonokami M. Terahertz wave polarization rotation with double layered metal grating of complimentary chiral patterns. Opt Express 2007;15:11117–25.
[163] Plum E, Zhou J, Dong J, et al. Metamaterial with negative index due to chirality. Phys Rev B 2009;79:035407.
[164] Zhou J, Dong J, Wang B, Koschny T, Kafesaki M, Soukoulis CM. Negative refractive index due to chirality. Phys Rev B 2009;79:121104.
[165] Decker M, Ruther M, Kriegler CE, et al. Strong optical activity from twisted-cross photonic metamaterials. Opt Lett 2009;34:2501–3.
[166] Zhang S, Zhou J, Park Y-S, et al. Photoinduced handedness switching in terahertz chiral metamolecules. Nat Commun 2012;3:942.
[167] Asadchy VS, Faniayeu IA, Ra'di Y, Semchenko IV, Khakhomov SA. Optimal arrangement of smooth helices in uniaxial 2d-arrays. In: 2013 7th International Congress on Advanced Electromagnetic Materials in Microwaves and Optics. 2013:244–6.
[168] Li M, Guo L, Dong J, Yang H. An ultra-thin chiral metamaterial absorber with high selectivity for LCP and RCP waves. J Phys D Appl Phys 2014;47:185102.
[169] Asadchy VS, Faniayeu IA, Ra'di Y, Khakhomov SA, Semchenko IV, Tretyakov SA. Broadband reflectionless metasheets: frequency-selective transmission and perfect absorption. Phys Rev X 2015;5:031005.
[170] Menzel C, Rockstuhl C, Lederer F. Advanced Jones calculus for the classification of periodic metamaterials. Phys Rev A 2010;82:053811.
[171] Mutlu M, Akosman AE, Serebryannikov AE, Ozbay E. Diodelike asymmetric transmission of linearly polarized waves using magnetoelectric coupling and electromagnetic wave tunneling. Phys Rev Lett 2012;108:213905.
[172] Huang C, Feng Y, Zhao J, Wang Z, Jiang T. Asymmetric electromagnetic wave transmission of linear polarization via polarization conversion through chiral metamaterial structures. Phys Rev B 2012;85:195131.
[173] Zhang S, Liu F, Zentgraf T, Li J. Interference-induced asymmetric transmission through a monolayer of anisotropic chiral metamolecules. Phys Rev A 2013;88:023823.
[174] Xu Y, Shi Q, Zhu Z, Shi J. Mutual conversion and asymmetric transmission of linearly polarized light in bilayered chiral metamaterial. Opt Express 2014;22:25679–88.
[175] Wang Y-H, Shao J, Li J, Zhu M-J, Li J, Dong Z-G. Unidirectional cross polarization rotator with enhanced broadband transparency by cascading twisted nanobars. J Opt 2016;18:055004.
[176] Wu L, Yang Z, Cheng Y, et al. Giant asymmetric transmission of circular polarization in layer-by-layer chiral metamaterials. Appl Phys Lett 2013;103:021903.
[177] Grady NK, Heyes JE, Chowdhury DR, et al. Terahertz metamaterials for linear polarization conversion and anomalous refraction. Science 2013:1235399.
[178] Cheng YZ, Withayachumnankul W, Upadhyay A, et al. Ultrabroadband reflective polarization convertor for terahertz waves. Appl Phys Lett 2014;105:181111.
[179] Ma HF, Wang GZ, Kong GS, Cui TJ. Broadband circular and linear polarization conversions realized by thin birefringent reflective metasurfaces. Opt Mater Express 2014;4:1717–24.
[180] Fernandes DE, Silveirinha MG. Optical tractor beam with chiral light. Phys Rev A 2015;91:061801.
[181] Ra'di Y, Asadchy VS, Tretyakov SA. Tailoring reflections from thin composite metamirrors. IEEE Trans Antennas Propag 2014;62:3749–60.
[182] Albooyeh M, Alaee R, Rockstuhl C, Simovski C. Revisiting substrate-induced bianisotropy in metasurfaces. Phys Rev B 2015;91:195304.
[183] Elliott R. On the theory of corrugated plane surfaces. IRE Trans Antennas Propagat 1954;2:71–81.

[184] Kraft M, Braun A, Luo Y, Maier SA, Pendry JB. Bianisotropy and magnetism in plasmonic gratings. ACS Photonics 2016;3:764–9.
[185] Odit M, Kapitanova P, Belov P, Alaee R, Rockstuhl C, Kivshar YS. Experimental realisation of all-dielectric bianisotropic metasurfaces. Appl Phys Lett 2016;108:221903.
[186] Shevchenko A, Kivijärvi V, Grahn P, Kaivola M, Lindfors K. Bifacial metasurface with quadrupole optical response. Phys Rev Appl 2015;4:024019.
[187] Albooyeh M, Simovski CR. Substrate-induced bianisotropy in plasmonic grids. J Opt 2011;13:105102.
[188] Yazdi M, Albooyeh M, Alaee R, et al. A bianisotropic metasurface with resonant asymmetric absorption. IEEE Trans Antennas Propag 2015;63:3004–15.
[189] Balmakou A, Podalov M, Khakhomov S, Stavenga D, Semchenko I. Ground-plane-less bidirectional terahertz absorber based on omega resonators. Opt Lett 2015;40:2084–7.
[190] Tretyakov SA, Viitanen AJ. Electromagnetic properties of periodical arrays with small nonreciprocal inclusions. J Electromagnet Wave 2000;14:1159–77.
[191] Wang Z, Wang Z, Wang J, et al. Gyrotropic response in the absence of a bias field. Proc Natl Acad Sci 2012;109:13194–7.
[192] Sounas DL, Caloz C, Alù A. Giant non-reciprocity at the subwavelength scale using angular momentum-biased metamaterials. Nat Commun 2013;4:2407.
[193] Degiron A, Smith DR. One-way glass for microwaves using nonreciprocal metamaterials. Phys Rev E 2014;89:053203.
[194] Mousavi SH, Khanikaev AB, Allen J, Allen M, Shvets G. Gyromagnetically induced transparency of metasurfaces. Phys Rev Lett 2014;112:117402.
[195] Lindell IV, Tretyakov SA, Oksanen MI. Conductor-backed Tellegen slab as twist polariser. Electron Lett 1992;28:281–2.
[196] Taravati S, Khan BA, Gupta S, Achouri K, Caloz C. Nonreciprocal nongyrotropic magnetless metasurface. IEEE Trans Antennas Propag 2017;65:3589–97.
[197] Hsu L, Dupré M, Ndao A, Yellowhair J, Kanté B. Local phase method for designing and optimizing metasurface devices. Opt Express 2017;25:24974–82.
[198] Popov E, Tsonev L, Maystre D. Gratings – general properties of the Littrow mounting and energy flow distribution. J Mod Opt 1990;37:367–77.
[199] Popovic Z, Mortazawi A. Quasi-optical transmit/receive front ends. IEEE Trans Microw Theory Techn 1998;46:1964–75.
[200] Hum SV, Perruisseau-Carrier J. Reconfigurable reflectarrays and array lenses for dynamic antenna beam control: a review. IEEE Trans Antennas Propag 2014;62:183–98.
[201] Yu N, Genevet P, Kats MA, et al. Light propagation with phase discontinuities: generalized laws of reflection and refraction. Science 2011;334:333–7.
[202] Kildishev AV, Boltasseva A, Shalaev VM. Planar photonics with metasurfaces. Science 2013;339:6125.
[203] Monticone F, Estakhri NM, Alù A. Full control of nanoscale optical transmission with a composite metascreen. Phys Rev Lett 2013;110:203903.
[204] Achouri K, Yahyaoui A, Gupta S, Rmili H, Caloz C. Dielectric resonator metasurface for dispersion engineering. IEEE Trans Antennas Propag 2017;65:673–80.
[205] Decker M, Staude I, Falkner M, et al. High-efficiency dielectric Huygens' surfaces. Adv Opt Mater 2015;3:813–20.
[206] Yu YF, Zhu AY, Paniagua-Domnguez R, Fu YH, Luk'yanchuk B, Kuznetsov AI. High-transmission dielectric metasurface with 2π phase control at visible wavelengths. Laser Photonics Rev 2015;9:412–8.
[207] Elsakka AA, Asadchy VS, Faniayeu IA, Tcvetkova SN, Tretyakov SA. Multifunctional cascaded metamaterials: integrated transmit arrays. IEEE Trans Antennas Propag 2016;64:4266–76.
[208] Chen M, Abdo-Sánchez E, Epstein A, Eleftheriades GV. Experimental verification of reflectionless wide-angle refraction via a bianisotropic Huygens' metasurface. 2017 XXXIInd General Assembly and Scientific Symposium of the International Union of Radio Science (URSI GASS). 2017:1–4.
[209] Epstein A, Eleftheriades GV. Arbitrary antenna arrays without feed networks based on cavity-excited omega-bianisotropic metasurfaces. IEEE Trans Antennas Propag 2017;65:1749–56.
[210] Wong JPS, Epstein A, Eleftheriades GV. Reflectionless wide-angle refracting metasurfaces. IEEE Antennas Wirel Prop Lett 2016;15:1293–6.
[211] Epstein A, Eleftheriades GV. Synthesis of passive lossless metasurfaces using auxiliary fields for reflectionless beam splitting and perfect reflection. Phys Rev Lett 2016;117:256103.
[212] Lavigne G, Achouri K, Asadchy V, Tretyakov S, Caloz C. Susceptibility derivation and experimental demonstration of refracting metasurfaces without spurious diffraction. IEEE Trans Antennas Propag 2018;66:1–1.
[213] Ra'di Y, Sounas DL, Alù A. Metagratings: beyond the limits of graded metasurfaces for wave front control. Phys Rev Lett 2017;119:067404.
[214] Li Z, Huang L, Lu K, Sun Y, Min L. Continuous metasurface for high-performance anomalous reflection. Appl Phys Express 2014;7:112001.
[215] Ho YZ, Cheng BH, Hsu W-L, Wang C-M, Tsai DP. Anomalous reflection from metasurfaces with gradient phase distribution below 2π. Appl Phys Exp 2016;9:072502.
[216] Díaz-Rubio A, Asadchy V, Elsakka A, Tretyakov S. From the generalized reflection law to the realization of perfect anomalous reflectors. Sci Adv 2017;3:e1602714.
[217] Mohammadi Estakhri N, Alù A. Wave-front transformation with gradient metasurfaces. Phys Rev X 2016;6:041008.
[218] Asadchy VS, Wickberg A, Díaz-Rubio A, Wegener M. Eliminating scattering loss in anomalously reflecting optical metasurfaces. ACS Photonics 2017;4:1264–70.
[219] Asadchy V, Daz-Rubio A, Tcvetkova S, et al. Flat engineered multichannel reflectors. Phys Rev X 2017;7:031046.
[220] Collischon M, Haidner H, Kipfer P, et al. Binary blazed reflection gratings. Appl Opt 1994;33:3572–7.
[221] Kwon D-H, Tretyakov SA. Perfect reflection control for impenetrable surfaces using surface waves of orthogonal polarization. Phys Rev B 2017;96:085438.